Joint Centre for Mesoscale Meteorology, Reading, UK

Multi-sensor synthesis of the mesoscale structure of a cold-air comma cloud system

K. Browning
P. Panagi
E. M. Dicks

Internal Report No. 112
NWP Technical Report No. 301

March 2000

Met Office Joint Centre for Mesoscale Meteorology Department of Meteorology
University of Reading PO Box 243 Reading RG6 6BB United Kingdom
Tel: +44 (0)118 931 8425 Fax: +44 (0)118 931 8791
www.metoffice.com

Designed and produced by the Met Office © Crown copyright 2001 01/0240 The Met Office logo is a registered trademark.

1 March 2000

Multi-sensor synthesis of the mesoscale structure of a cold-air comma cloud system

By K.A.BROWNING*, P.PANAGI and E.M.DICKS

University of Reading, UK

Summary

A multiscale study of a cold-air comma cloud that produced an area of heavy rain and locally severe weather has been undertaken by synthesizing data from a research microwave Doppler radar and VHF and UHF Doppler wind profilers, along with routinely available radar-network, satellite, in situ and mesoscale-model data. The rain area was generated in the exit region of an upper-level jet characterised by laminated velocity perturbations. Some of the perturbations were attributable to inertia-gravity wave activity. The rain area itself is shown to have been composed of a well organized set of mesoscale rainbands each being due to a mixture of upright and slantwise convection. The existence of the multiple rainbands may have been related to the multi-layered atmospheric structure upwind. Each of the rainbands had cold-frontal and warm-frontal portions, so as to form a series of mini warm sectors stacked along the axis of the comma cloud at roughly 70km intervals. The multiple rainbands were accompanied by multiple fingers of overunning low – θ_w air from part of a dry intrusion originating from just below a major tropopause fold. The fold contained an intense potential-vorticity maximum which appeared to be the focus of the overall system. The operational Met Office mesoscale model, with its 12 km grid, is shown to have resolved many but not all of the key features of the rainbands. It is argued that further improvements in forecasting important local detail could be achieved by further increasing its resolution.

Key words: Mesoscale rainbands, comma cloud, weather radar, wind profiler, mesoscale model.

* Corresponding author: Joint Centre for Mesoscale Meteorology, Department of Meteorology, University of Reading, PO Box 243, Reading RG6 6BB, UK.

Sub-synoptic scale troughs and cyclones which form on the cold-air side of the main polar front are often responsible for adverse weather. Some of the more vigorous systems contain convective rainbands that can produce locally severe weather, including thunderstorms, with strong wind gusts and small tornadoes. There has, however, been relatively little research into the mesoscale organization of these convective features and how they relate to the larger-scale dynamics of the overall comma-cloud system. The rainbands (but not the embedded convection) occur on a scale that is just about resolvable by the finest scale operational numerical weather prediction (NWP) models. With further improvements in model resolution, as well as in model physics and data assimilation, there may be an opportunity to make very-short-range forecasts of such events more site-specific and therefore more economically beneficial than at present. In order to determine the best way forward, it is helpful to obtain a deeper understanding of the mesoscale sub-structure and processes in these weather systems. This provides the practical motivation for the present study in which we use multiple data sources to carry out a multiscale description of a vigorous cold-air comma cloud that affected the British Isles on 26 January 1999. We also make use of the mesoscale version (12 km grid) of the UK Met Office's Unified Model and find out just how much of the observed mesoscale structure it was capable of reproducing in its present operational form.

There is still some confusion over terminology for cold-air comma-cloud systems. This is an indication of the imperfect state of our understanding. Heinemann and Claud (1997) have proposed that such systems in general should be referred to as polar mesocyclones but that, if they are less than 1000 km in scale and have surface winds in excess of 15 ms^{-1}, they should be referred to as polar lows. The system investigated in this paper narrowly falls into the latter category although, because of the great intensity of upper-level forcing in this case, it probably does not correspond to what UK meteorologists would traditionally choose to call a polar low.

A helpful subcategorization of polar mesocyclones was provided by Businger and Reed (1989) who classified them into three types according to whether they occur in association with (i) a short-wave/jet-streak, (ii) an arctic front or (iii) an old cold low. It is the first of these categories that gives rise to cold-air comma clouds of the kind described in the present

paper. Reed (1979) summarizes the attributes of cold-air comma clouds associated with jet streaks as follows:

- The comma cloud lies in a region of appreciable baroclinicity as judged by the 1000-500 mb thickness and it is located on the cold side of the baroclinic zone where the lapse rate is conditionally unstable through a considerable depth.
- The comma cloud is typically 1000 km in the direction normal to the polar front and 500 km in the parallel direction.
- A surface pressure trough lies under the trailing edge of the comma tail and, in the more intense cases, a surface low develops under the comma head.
- The notch of the comma lies in the region of strong horizontal shear (cyclonic vorticity) on the poleward side of the jet stream axis at 500 mb.

Reed (1979), and also Mullen (1979), thus concluded that the above comma-cloud systems are primarily baroclinic phenomena as proposed by Harrold and Browning (1969). Conditional instability of the second kind and barotropic instability may also contribute to their formation. Their small size is attributable in part to the effect of the small static stability at low levels. As Businger and Reed (1989) point out, this class of comma cloud should not be confused with the much larger comma-cloud pattern accompanying mid-latitude frontal cyclones (Carlson 1980). A schematic diagram showing the typical relationship of a cold air comma cloud to a major frontal cyclone and upper-level jet streak is shown in Fig. 1.

Amongst the few existing studies of the mesoscale substructure of cold-air comma clouds are those carried out in the Pacific Coast region of Washington State. Locatelli et al (1982) observed warm frontal and cold frontal rainbands similar to those encountered in normal frontal systems. Businger and Hobbs (1987), using dual Doppler and aircraft measurements, identified multiple rainbands associated with a tongue of warm air and a low-level jet ahead of the trough. The rainbands had tops between 4 and 9 km and a wavelength of about 50 km. They contained convective elements with updraughts of several ms^{-1} originating in the boundary layer. Associated precipitation cores retained their identity and strength over periods of several hours. Convective updraughts were also observed near the tops of the rainbands; these produced ice crystals that grew by riming and aggregation at lower levels.

The comma cloud analysed in the present paper, situated in the exit region of an upper-level jet streak, was also characterised by multiple convective rainbands. Those studied by Businger and Hobbs (1987) were dissipating when they passed through the Pacific Coast observational network and radar reflectivities were mainly less than 40 dBz. By contrast, the comma cloud system discussed in this paper, which formed just upwind of Ireland, was in the developing-to-mature stage and producing rather more intense precipitation as it passed over the observational facilities in England and Wales. Our study lacks the dual Doppler and aircraft facilities of the Pacific Coast study but it benefits from high-resolution data from the single Doppler radar at Chilbolton and continuous wind profiles from the VHF radar at Aberystwyth and the UHF wind profiler radar at Camborne. All these radars were well situated with respect to the track of the comma cloud system. Our study also benefits from multi-channel imagery from the satellite Meteosat and broad coverage from the UK weather radar network which revealed almost the entire series of mesoscale rainbands that characterised the comma cloud. Detailed output is also used from the operational Met Office mesoscale model which itself was benefiting from assimilating the high-density routine observations over the UK (MacPherson et al 1996), including hourly wind profiles from the radar at Aberystwyth.

The paper is structured as follows. Section 2 outlines the principal sources of data. Section 3 describes the dynamical context, which was dominated by a small but intense maximum of potential vorticity (PV) that descended to low levels within a deep tropopause fold beneath a strong northwesterley jet. Section 4 describes the 3-D mesoscale substructure of the resulting comma cloud and the associated multiple rainbands. The comma cloud occurred in the region of ascent ahead of the PV maximum, or to put it another way, in association with the indirect ageostrophic circulation at the exit of the upper-level jet. Section 5 uses observations from the VHF and UHF radars to describe the vertical structure of this jet exit region. Section 6 then uses output from the mesoscale model to show the influence of overunning dry air, with low wet-bulb potential temperature (θ_w), on the structure of the rainbands. The results of the preceding sections are then synthesized in Sec. 7. and the capability of the model to reveal important mesoscale features is assessed in Sec. 8. Conclusions are given in Sec. 9.

2. Data sources

(a) Observations

This is primarily an observational study, benefiting not only from routinely available in situ, satellite and radar network data, but also from special high-resolution data from three other radars:

The Chilbolton Radar

The radar at Chilbolton (51.15°N, 1.44°W) is a 3GHz (10cm wavelength) advanced research radar (Goddard et al 1994). In addition to providing Doppler velocities and reflectivity measurements, it is capable of providing a variety of polarisation measurements. The radar has a peak power of 560 kW and, together with its sensitive receiver and high-gain 25m-diameter dish, this enables it to detect virtually all significant precipitation out to the 100 km range used in the present study. The 25m diameter of the dish gives it an angular resolution as small as 0.3°, corresponding to 50m at 100 km range The data have a range resolution of 300m, achieved by range-averaging over groups of four gates, each 75m in length. In this study the radar was scanned in the vertical, in RHI (Range Height Indicator) mode, at different azimuths to reveal the 3-D distribution of precipitation and to provide velocity information on the scale of an individual rainband. Information on the variation in bright-band height, which was especially clear from the measurements of linear depolarisation ratio, was used to identify local regions of strong horizontal temperature gradient.

The Aberystwyth radar

The VHF wind profiling radar at Aberystwyth (52.4°N, 4.0°W, altitude 90m) is referred to as an MST radar because it can make measurements in the Mesosphere Stratosphere and Troposphere; however, we shall use it only in the troposphere and lower stratosphere where it detects backscatter from refractive index gradients on scales of about 3m (equal to half the radar wavelength). It operates at 46.5MHz, with peak power 160 kW and has an antenna area of 10^4 m^2. A full description may be found in Slater et al (1991). A pulse length of 8μs was used, phased-coded with 2μs segments corresponding to a range resolution of

300 m. The beam was successively steered to the vertical, SE6. SE12, NE6, NW6, and NW12 directions (SE6 means 6° zenith angle towards the south-east) with dwell times of 20s; spectra for a particular direction were averaged before processing. The primary products of the radar used in this study are time-height patterns of the vertical echo power and wind components derived from the SE6, NE6 and vertical beams. Each cycle of measurements from these beams takes 1.5 min to acquire; winds can be derived with an accuracy of 1.2 m s^{-1} (standard deviation) for 12-minute average spectra (Astin and Thomas 1991).

The Camborne radar

The UHF radar at Camborne (51.13°N, 5.10°W) is a commercially available Radian LAP-3000 wind profiler. It uses a four-panel antenna, with a 915 MHz radar operating in three-beam mode: vertical, north and east at 23.5° from zenith. The beam has a 10° half-width. The principle of operation of the Camborne wind profiler is similar to that of the MST radar except that it operates at a wavelength for which it receives detectable clear-air returns only in the lowest 2 to 4 km of the atmosphere. However, unlike the MST radar, it also detects precipitation and where this occurs its vertical coverage can be extended. Operationally 40 measurements obtained at 45-second intervals are averaged to provide highly reliable measurements. However, to obtain mesoscale detail in the present study, the data were averaged over much shorter (4.5 minute) periods.

(b) Mesoscale model

The UK Meteorological Office Unified Model (UM) (Cullen, 1993) is a hydrostatic spherical grid-point model. The current mesoscale version of the UM has a 146 x 182 point horizontal domain, and a vertical 38-level hybrid sigma-pressure coordinate. The horizontal grid spacing is 0.11 deg x 0.11 deg equating to an approximate 12km resolution, The model is run operationally four times a day, assimilating data from a dense observational network (MacPherson et al 1996, Lorenc et al 1991), and produces analyses and hourly forecasts for each run. Boundary forcing is from the operational forecast UM at global resolution (432 x 325 x 30 grid points, 60 km spacing). The basic prognostic variables, p*,T,u,v,omega,q, required for deriving the various diagnostics, are

re-mapped from the vertical hybrid coordinate to constant 50 mb pressure surfaces between 1000mb and 50 mb, and then the diagnostics computed (Panagi & Dicks, 1997).

3. The dynamical context

The cold-air comma cloud that is the subject of this case study can be seen over England and Wales in Fig. 2. This is a water vapour (WV) image for 1230 UTC[X]. Upper-tropospheric dry air is shown dark, and moist air and cloud is shown pale grey. The grey scale has been selected to highlight striations in the cloud top, orientated roughly northwest-to-southeast with a mean spacing of 70km, an order of magnitude greater than the image resolution. These striations are related to the mesoscale rainbands discussed in Sec. 4. The comma cloud is situated ahead of the ridge, on the cold-air side of the large-scale trough-ridge pattern delineated in the imagery (Fig.2) by the major undulation in the pattern of upper-level moisture and cloud. The axis of the large-scale trough extends down from the west coast of Norway to northwest Spain. The axis of the ridge is located in mid-Atlantic, at about 25°W. The axis of the upper-level northwesterly jet ahead of this ridge is colocated with the leading edge of moist air aloft (grey) which contains a streak of cirrus (light grey) where it crosses the tail of the comma cloud just off the southwest tip of England. As we show later, the tail of the comma cloud extended westwards as a shallow feature just south of Ireland but this is not evident in the WV imagery which is dominated by radiation emitted from higher levels in the troposphere.

Behind the comma cloud, over the Irish Sea, Fig.2 shows a small WV 'dark zone' (Weldon and Holmes 1991). This was due to a downward intrusion of dry stratospheric air. As we shall show, it was also characterised by high values of potential vorticity coming down to low altitudes. The dark zone developed from a weak feature first detected near 56°N 18°W at 0 UTC. By 06 UTC it was just west of Ireland at 54°N 11°W, with the comma cloud itself developing over Ireland. According to the Met Office Global Model (not shown), the main period of descent for the stratospheric air was between 06 and 12 UTC. At 500 mb the maximum value of PV was about 1 PV unit at 0 and 06 UTC but by 12 UTC, because of the descent of the stratospheric air, it had increased to over 2 PV units.

[X] All times refer to 26 January 1999

Figure 3 shows the main synoptic features of the comma cloud system at 12 UTC as given by the mesoscale model. Figure 3(a) shows the mean-sea-level pressure and the axis of the comma-cloud trough. There was no closed circulation at this time but a small closed low formed in the northern Irish Sea at 13 UTC and travelled to the east coast of England (Norfolk) by 18UTC. Figure 3 (b) shows two key features of the circulation, namely an upper-level jet centred at 300 mb and a low-level jet centred at 800 mb. The low-level jet was part of an indirect ageostrophic circulation at the exit of the upper-level jet as discussed by Uccellini and Johnson (1979). This circulation advected moist air with high θ_w northeastwards ahead of the axis of the comma trough (see the 281K isopleth in Fig 3(a); a tongue of air with θ_w = 279K reached as far as north Wales but is not shown because of its convoluted structure elsewhere within the model domain).

The left-hand edge of an upper-level jet is a region of high vorticity and potential vorticity (PV). The associated strong local PV maximum over NE Ireland at 12UTC descended within the upper part of a tropopause fold that trailed down towards the west underneath the upper-level jet. The effect of this PV maximum can be seen in Fig.4 which shows several fields within the 295K (dry) isentropic surface, chosen to intersect the PV maximum. The thin solid contours show the geopotential height of this surface at 500 m intervals. In the region of interest, ahead of the ridge on the western side of the large-scale trough, the surface slopes downwards to the southwest. The surface is actually within or very close to the tropopause fold and it is near the top of the region of moist ascending air that was giving rise to the comma cloud (see dashed isopleth in later Fig. 15(e)).

Wind vectors in Fig. 4, plotted relative to the motion of the PV maximum, show a cyclonic circulation around the PV maximum. Since the flow is within a surface that slopes upwards toward the northeast, this is consistent with ascent in the southwesterly flow ahead of the PV maximum and descent behind it. This in turn is consistent with the model's own vertical velocity pattern (the thick isopleths show a region of ascent over 5 cm s^{-1} centred over southwest Wales and a region of descent over 5 cm s^{-1} to the northwest of Ireland). In other words, air in the tropopause fold was descending upstream of the PV maximum and ascending downstream of it. A similar circulation was induced within the cold air beneath the tropopause fold. The low-level jet shown in Fig. 3(b) was part of this circulation; this was part of the ascending flow that gave rise to the cloud and precipitation structure described in the next section.

4. Observed mesoscale substructure of the comma cloud and precipitation

(a) Multiple rainbands

Figures 5 (a) and (b) show the precipitation distribution associated with the comma cloud at 1515 and 16 UTC as obtained from the UK weather radar network. The rainfall is extensive and heavy in places, and distributed very unevenly in association with a series of curved convective rainbands. Fourteen of these are identified in Fig. 5 (a). Apart from Rainband No. 5, most can also be identified in Fig.5(b), as indeed was the case throughout the period 14 to 17 UTC when the bands were studied closely. Their spacing was typically 70 km (more between Nos. 7 and 8; less between Nos. 11,12,13 and 14). This is comparable with the spacing of the striations at cloud top as seen in the WV image in Fig. 2. The curved nature of the rainbands is such that their eastern ends (not Nos 1 & 2) tend to have a nearly north-south orientation (strictly NNW-SSE) in accordance with that of the cloud-top striations in the WV image. The western ends of the rainbands, however, trail off towards the west. The precise nature of the along-band transition in rainband structure is clarified a little later when we examine the detailed structure of one of them as it passed over the Chilbolton radar; however, a preliminary indication of their structure is given by the Meteosat images in Fig. 6.

Whereas the radar pictures in Fig.5 were selected to correspond to the time when the precipitation was close of the Chilbolton radar (cf Sec.4(b)), the satellite images in Fig. 6 are for the slightly earlier time of 14 UTC. This time was chosen for the clarity of the images in revealing the clouds responsible for the rainbands. Even so, it was still necessary to select the colour enhancements carefully in order to achieve this, especially for the visible image in Fig.6(a). What Fig. 6(a) shows is a series of curved cloud bands, the eastern ends of which are orientated nearly north-south and the western ends trail off to the west as for the precipitation bands. The infrared image in Fig.6(b) shows that the parts of the cloud bands with nearly north-south orientation occur where the cloud tops are colder than 230K (higher than 7km). The trailing parts to the bands, where they extend to the west, correspond to cloud tops that lower progressively so that their tops over extreme southwest Wales, for example, are close to 265 K (ie below 4 km).

(b) Substructure of one of the rainbands as derived from the Chilbolton radar

Rainband 7 travelled over the research radar at Chilbolton while the latter was performing systematic RHI scans, giving reflectivity, Doppler and polarization data as explained in Sec. 2. The structure of this rainband, synthesized from the Chilbolton radar, is depicted in Fig. 7. The figure shows the following characteristics:

- A *mesoscale warm sector* bounded by a sharp drop in θ_w along the cold-frontal portion and a gentler fall in θ_w in the warm-frontal region. The fall in θ_w was deduced from the change in height of the radar bright band, detected most clearly within the linear depolarization data (not shown), and it applies strictly to a level between 400 and 1000m. Much of the reduction in θ_w is seen to have been confined to a narrow strip behind the mesoscale cold front, with a partial recovery in θ_w behind. This is consistent with other evidence given shortly which suggests that this strip of cold air was due to the descending part of an ana-cold frontal circulation where dry air was descending from the rear and would have been cooled by evaporation and melting of the precipitation falling from the ascending part of the circulation (eg. Yang and Houze 1995).
- A *narrow cold-frontal rainband* (Houze, 1981; Browning 1990) along the line of the sharp temperature drop. This is associated with a typically 3km -wide band of 40 dBz echo with tops rising from 1km at the southwestern end (A) to 4km close to the northeastern end (B).Maximum reflectivities correspond to a rainfall intensity of about 80mm h^{-1}.
- A *wide frontal rainband* within which the narrow cold frontal rainband is embedded. It starts in the west as a cold-frontal rainband and terminates in the east as a warm-frontal feature. The band of radar echo is 30km wide with tops typically 3 km high near A, increasing to 60km wide, with tops to between 6 and 7 km, near B. The extent of echo decreases somewhat at lower levels owing to evaporation; this effect is especially pronounced just behind the deepest (most intense) part of the narrow cold frontal rainband, presumably because of stronger low-level descent here.

Figure 7 was derived from vertical (RHI) scans at 20-deg intervals. Data from three of these scans are displayed in Fig.8. Figures 8 (a), (b) and (c) show the radar reflectivity in different parts of Rainband 7: (a) shows the broad area of stratiform precipitation in the warm frontal region due to relatively uniform slantwise ascent: (the appearance on the radar network display (Fig. 5(b)) of a band of heavy rain in this region is an artefact because the network radars were detecting an intense bright band). (b) shows the convective narrow cold frontal rainband where it was most intense. Ahead of it, the bright band is at 1 km: behind it drops to ½ km. The Doppler display corresponding to (b) (not shown) depicts strong convergence below 1km and divergence above 1.5 km in the region of the narrow cold frontal rainband, and a classical ana-cold frontal circulation as depicted in Browning (1990:Fig 8.8). (c) show the mainly light rain (blue) associated with the wide cold frontal rainband, looking obliquely along its length, with the narrow cold frontal rainband (yellow) being intersected at 70 km range. The narrow cold frontal rainband in this region is weak and shallow. The wide cold frontal rainband is seen (Fig.8(c)) to be composed of many precipitation streamers evidently associated with upper-level convection due to the overunning low $-\theta_w$ air discussed in Sec. 6. The Doppler shear display in (d), corresponding in azimuth and time to the reflectivity plot in (c), shows an inclined shear layer (red) within the lower part of the precipitation system; this marks the interface between rearward-sloping ascent (above) and forward-sloping descent (below). We interpret these structures later within the context of the detailed mesoscale model results in Sec. 6(c).

5. Observed mesoscale substructure of the jet-stream exit region

The location of the multiple rainbands in relation to the upper-level flow is summarized in Fig. 9. This shows the family of mesoscale rainbands along the axis of a tongue (WW) of maximum θ_w curving around the exit region of an upper-level jet streak. Figure 9 is based on the structure at 16 UTC but portions of rainbands have been added (notably Rainband 5 and extensions to Rainbands 2, 3,4 & 6) to indicate features that had existed an hour or more previously. The spacing of the bands along the axis of the warm tongue (WW) was up to 70 km but the spacing decreased in the trailing cold-frontal parts of these bands. The individual rainbands were travelling almost due east and (except for Rainband 5) they tended to be persistent, those at the northern end eventually decaying as the axis WW of the overall system progressed with a component to the southeast. Immediately behind this, the upper-level jet was also travelling towards the southeast as shown by the open arrow in Fig.9. We

shortly examine the fine structure of the atmosphere as the rainband and jet-stream systems travelled over the MST radar at Aberystwyth (location A in Fig. 9). Taking into account the different directions of travel of the individual rainbands and the upper-level jet, it can be seen that the northernmost tip of Rainband 5 and the cold-frontal part of Rainband 4 would have passed overhead (at about 12 to13 UTC and 14 UTC, respectively), whilst the jet core would have remained almost overhead for several hours after 16 UTC.

The time-height sections derived from the MST radar at Aberystwyth are shown in Fig. 10. Time is plotted backwards in these sections and so, to a first approximation, they can be thought of as spatial cross-sections (allowing for the duality of travel directions mentioned above). Radiosonde ascents at nearby Aberporth (60km southwest of Aberystwyth) are presented later in Fig.11 to aid in the interpretation of Fig 10. Figure 10(a) depicting the wind strength, shows the upper-level jet (J) at 9.2km (300 mb) reaching Aberystwyth at 16 UTC. Ahead of the jet, the wind speed drops abruptly to 45 ms^{-1} within 2 hours (just over 100 km). A little farther ahead, between 9 and 13 UTC, there are patches of locally stronger winds corresponding to the upper part of the comma cloud. The axes of these stronger winds are indicated by the solid lines drawn on Fig.10(a) ; these are mainly between 7 and 8 km but rise above 8km between 12 and 13 UTC when the convection associated with Rainband 5 passes overhead (perhaps accounting for a noisy signal at 1230 UTC that has been excluded from the analyses). The region of the main jet stream after 15 UTC is characterised by layered wind fluctuations the axes of which are highlighted by dotted lines. Layers with weak fluctuations also exist at low levels between 1030 and 17 UTC but they do not show up clearly in Fig. 10(a).The wind fluctuations in this region are more evident in the westerly wind component shown in Fig.10(b).

A layered pattern can also be seen in the 1.5-minute resolution plot of radar power in Fig.10 (c). Here the warm colours represent strong signals due to Bragg scattering from layers of strong static stability, and/or strong humidity gradients in the troposphere. Some of the significant features in Fig. 10(c) are as follows:

- The echo layers above 9 km highlighted by dotted lines, before 9 UTC and after 14 UTC, correspond to the main tropopause. In particular the letter T plotted at 17 UTC corresponds to the tropopause as observed at that time by the nearby Aberporth radiosonde (Fig.11(b)). (The almost horizontal layer near 7 km before 6UTC

appeared from the 06 UTC radiosonde (not shown) to be like a secondary tropopause).

- Between 9 and 14 UTC the main tropopause became indistinct, as is typical in the vicinity of a tropopause fold (Vaughan et al 1995). The layer of strong echo centred near 8 km and highlighted by the solid line between 8 and 13 UTC, was directly above the comma cloud. Fig. 11(a), depicting the 12 UTC radiosonde at nearby Aberporth, shows that the base of this echo corresponded both to a sharp gradient in humidity and to the base of a very stable layer where the comma cloud was penetrating into lowered stratospheric air ahead of the jet and creating its own sharply defined tropopause. The 2-km thick cap of strong echo above the comma cloud shows the extent of the strong refractivity inhomogeneities probably due to the dispersion of gravity waves above the comma cloud.
- The inclined layers, highlighted in Fig.10(c) by the dotted lines below the upper jet, are parellel to the velocity fluctuations shown by the sloping lines in Figs.10(a) and (b). The longest and most intense layer echoes, sloping gently downwards after 15 UTC, correspond to a strong frontal zone as shown by the symbols X in the 17 UTC Aberporth sounding (Fig.11(b)) and the later 23 UTC sounding (not shown). Time-height output from the mesoscale model shown later (Sec.6) indicates a close correspondence between this frontal zone and a deep tropopause fold with high PV.
- The intense jagged echoes, mainly below 3km, show what are believed to be the edges of upward excursions of moist boundary-layer air. Most of these are relatively small excursions; however, the bigger, more smoothly sloping, ones highlighted by solid lines between 1230 and 1430 UTC are thought to correspond to more organized slantwise convection associated with Rainbands 4 and 5. Between 12 and 1230 UTC, at the leading edge of these layers, a vertical-windshear plot derived from the MST radar (not shown) was very noisy up to 7 km, indicating the passage of deep upright (buoyant) convection probably associated with Rainband 5; this is shown by the vertical arrow in Fig.10(b).

The cause of the laminated structure in the jet-streak region may be inertia-gravity waves due to geostrophic adjustments in the jet exit (Thomas et al 1992). This would be consistent with the MST wind hodographs in Figure 12 which reveal a pronounced looped structure in which the perturbation wind vector rotates clockwise with height above the tropopause (Fig.12(a)) and anticlockwise below the tropopause (Fig.12(b)). The vertical wavelength, as

also shown by the radar-observed laminations in Fig.10 and the variations in dew point (and dew-point depression) in Fig.11(b), is between 1 and 3 km, and this too would be consistent with inertia-gravity waves.

The jet-streak related laminations observed by the MST radar were situated behind the rainbands but they were not well defined at low levels very close to the rainbands. Clearer evidence of laminated structures coexisting at low levels in close proximity to rainbands is contained within data from the UHF wind profiling radar at Camborne in southwest England. The sequence of rainbands 8 to 14 passed over Camborne between 1245 and 1630 UTC. The profiler there detects echoes from both the clear air and from precipitation particles. The time-height section of echo power in Fig.13 shows intense columnar echoes associated with the passage of the shallow and rather convective rainbands embedded within a background of weaker layer echoes due to humidity and temperature laminations. The latter are emphasised by a scalloped line where it is believed to correspond to the top of the boundary layer and by dotted lines where they are thought to correspond to inclined stable layers. These stable layers most likely correspond to the laminated wind perturbations and we are led to speculate that the wind perturbations, acting in a region of horizontal θ_w- gradient, might generate regions of enhanced potential instability and thereby influence the generation of the convective rainbands. For technical reasons we were unable to extract high-resolution winds from the UHF radar; however, wind hodographs from the Aberystwyth MST profiler at levels below 7 km (not shown) display only minimal looping behaviour (diameter of loops <2 m s^{-1}) and so it is difficult to prove that the laminations at low levels are caused by the inertia-gravity-wave induced wind fluctuations. Whatever their cause, we cannot dismiss such perturbations as unimportant since even a difficult-to-detect perturbation of 1 m s^{-1} acting consistently for many hours may have had a significant effect on the thermal structure. This may be related to the model-generated fingers of overrunning dry air (discussed in Section 6).

6. Model-derived mesoscale substructure of the jet streak and comma cloud system.

(a) Mesoscale model time-height sections over Aberystwyth

Time-height sections have been derived from the mesoscale model for the grid-point location nearest to the MST radar at Aberystwyth (52.44°N, 3.96°W, terrain height 178m). The resulting fields of wind speed (u-component), relative humidity and potential vorticity are

plotted in Figs.14 (a),(b) and (c), respectively. They are constructed from a set of four 6-hour sequences of hourly forecasts using runs starting at 0, 6,12 and 18UTC. The first of the sections (Fig.14(a)) shows model-based isotachs superimposed on a simplified monochrome version of Fig.10(b): the broad agreement between the two is quite good and, indeed, the purpose of showing it is to give confidence in the performance of the model so that other model results may be used with confidence.

The dominant feature evident in Figs.14(b) and (c) is the tropopause fold beneath the upper-level jet core. It shows up in (b) as a very dry layer, with relative humidity less than 20%, extending all the way down to 3 km at 23 UTC. In (c) it is revealed as a region of high PV, with values as low as 2 PV units, corresponding to stratospheric air, extending down to 4 km at 22 UTC and values between 5 and 6 PV units extending down to almost 5 km at 15 UTC. Radar-detected features from Fig.10 (c) are superimposed on Figs.14(b) and (c). They show a generally good correspondence between the model and radar-inferred locations of stratospheric air.

Of particular interest in Fig.14(c) is the close proximity of the region of dry air with anomalously high PV (in the tropopause fold) to the region of moist air ascending beneath it within the comma cloud. This had two consequences. Firstly the PV maximum within the fold is likely to have been playing a dominant role in forcing the overall comma-cloud circulation. Secondly, as elucidated in the following subsections, some of the dry, relatively low $-\theta_w$, air at the base of this PV maximum was entering the comma-cloud circulation and creating potential instability by overrunning high $-\theta_w$ air at lower levels. This gave rise to the strongly convective nature of this event, (the MST-radar derived feature represented by solid lines at 1230 UTC in Fig.14 (b and c) correspond to this convection). We now examine the overrunning process in some detail.

(b) Mesoscale model representation of the overrunning dry low $-\theta_w$ air.

Figure 15 shows several model sections through the comma-cloud system at 16 UTC. Figures 15(a) and (b) are plan sections at 800 and 600 mb, respectively. They draw attention to the band of saturated air (shaded) along the axis of the comma cloud which is wider aloft than near the surface. Figure 15(e) shows a vertical section (BB) derived by fitting a spline along the axis of the saturated region. It shows the saturated region to be characterised by a

roughly wet adiabatic lapse rate, situated beneath a dry stable layer, the base of the latter ascending from 700 mb near B to 400 mb near B^1. The dry air is associated with the tropopause fold (see the PV=1 contour); pockets of dry air also intrude beneath the main tropopause fold into the top of the saturated region. Figure 15(b) shows the dry air approaching the saturated region from the west, and Fig.15(c) shows how fingers of this dry air penetrate increasingly into the saturated region with time. The most pronounced of these fingers, labelled D7 (Dry Intrusion 7), occurred on the southern flank of the vigorous rainband, Rainband 7, (it relates to the rain-free strip seen in Fig. 5(b) along the south coast of England). Figure 15(c) also shows three other fingers of dry air to the north of D7; they occur in the region of Rainbands 1 to 6 but do not correspond with them in a one-to-one manner. These fingers of dry air are characterised by a low θ_w and they generate potential instability in a layer above 700 mb.

The overrunning of low $-\theta_w$ air above 700 mb, indicative of kata-cold frontal structure, occurred to a greater or lesser extent along the whole length of the comma cloud. It was responsible for much of the convective precipitation: see, for example, the observed upper-level convective cells in Fig.8(c). Individual rainbands appear to be associated with fingers of more strongly overrunning air. Similar fingers accompanying convective rainbands were reported by Browning and Golding (1995).

(c) Identification of both ana- and-kata-circulation in Rainband 7

Although the correspondence between individual overunning dry fingers in the model and observed mesoscale rainbands is only partial, it was particularly good for Rainband 7. This rainband was of special interest not just because it was well observed and modelled (Sec. 4(b)) but also because it manifested a combination of circumstances in which an ana-cold frontal circulation (ie forward-sloping descent undercutting rearward-sloping ascent) occurred below 700 mb *at the same time* that overrunning was occurring aloft (katastructure). This was evident in Doppler radar sections such as Fig.8(d) which shows the shear zone, separating the forward-sloping descent from the rearward-sloping ascent, extending down from 2 km to the ground. The corresponding reflectivity pattern in Fig.8(c) shows a decrease in reflectivity in the snow below the shear zone, indicative of evaporation in the low-level forward-sloping descent. And, as mentioned earlier, Fig.8(c) also shows mid-level convective cells above 3 km, indicative of the low $-\theta_w$ air overrunning aloft. This same combination of

ana-and kata-structure was indeed reproduced by the model. The rear edge of the dark shading in Fig.15(a) shows the rear edge of the saturated air at 700 mb due to the rearward-sloping ana-ascent. The extent of the dark shading shows that, consistent with the underlying forward-sloping descent, the rear edge of the saturated air at 800mb is situated up to 50km farther ahead. This sloping moisture boundary is evident in the cross-section AA shown in Fig. 15(d). The rear edge of the models' cloud associated with the ana-circulation is situated at 700mb at x = 90 km and dry air can be seen in Fig. 15(d) overrunning it as part of the main kata-circulation as far ahead as x = 250 km at 650mb. Ahead of this the main cloud band extends all the way up to 400 mb.

The position of the Chilbolton radar is plotted (X) in Fig.15(a). If one shifts the model fields 60km to the east to allow for a small overall positional (timing) error, then there is good agreement between the observed 3-D pattern of precipitation plotted in Fig.7 and the pattern of saturated air in the model. In particular the saturated region associated with the ana-cold frontal structure shown in the model just south of the Bristol Channel (Fig.15(a)), which is overrun by dry air above 700 mb (Fig.15(d)), corresponds to the shallow precipitation shown in Fig. 7 along the tail of the rainband. And the region of supersaturation (w.r.t. ice) in the model shown on the north-east side of the dry intrusion D7 in Fig.15(b) corresponds to the region in Fig.7 where precipitation extends up to 6 or 7 km (400 mb).

The ability of the model to reproduce these mesoscale humidity structures is reassuring, but it should be stressed that the velocity perturbations that generated them were very weak. The model's transverse circulation (not shown) responsible for generating the rearward-sloping saturated layer between 400 and 500 km in Fig.15(d) was only $\pm$ 1 ms^{-1}. A better defined feature of the model's velocity pattern was the low-level jet (LLJ) which extended along the axis of the overall comma cloud; it had a maximum component normal to the section AA of 22 ms^{-1} (see Fig.15(d)). The left (western) side of the LLJ corresponded to the location of the observed line convection, but of course the model was unable to reproduce this sub-grid scale phenomenon. The model was also unable to reproduce the abruptness of the observed drop in θ_w (from 278 to 275K) at the line convection. A concentrated θ_w - gradient did occur in the model (not shown) but the change (from 280 to 277K) was spread over 100 km or more; the radar showed a local sharp drop at the line convection followed by an (initial) rapid recovery. Diabatic processes, leading to a mesoscale rear-inflow jet and a local downdraught, were presumably responsible for the discrepancy.

7. Synthesis of the multiscale organization derived from the different analysis perspectives.

We have presented a detailed case study of a cold-air comma cloud which gave intense precipitation over England and Wales on 26 Jan 1999. The study concentrates on the period 12 to 16 UTC during which the comma-cloud system developed a small closed surface low. The opportunity is taken to study this case in particular detail because it passed over not only the UK weather radar network but also the research radars at Aberystwyth and Chilbolton during which time it was characterised by distinctive mesoscale substructure. The comma-cloud system, although quite intense, was by no means exceptional and the study is thought to give good insight into this general type of weather system. A special feature of the study is the synthesis of a variety of data sources. This enabled the structure of the weather system to be viewed from several perspectives which, when put together, provide unique insight into its multiscale organization.

The traditional synoptic perspective.

The comma cloud was situated in the cold air beneath a strong warm frontal zone and northwesterly jet stream. It formed in the exit region of an upper-level jet streak within the tropospheric part of an indirect transverse ageostrophic circulation. Part of this circulation was characterised by a low-level jet, with a relative flow toward the northeast at right angles to the jet axis. Although situated in the cold air, the flow was in a region of significant baroclinicity, and it caused the advection of a tongue of relatively high θ_w. The ascent of this tongue of air was responsible for the comma cloud and associated precipitation.

The PV perspective

The upper-level jet streak was associated with a strong potential-vorticity maximum, which was embedded within stratospheric air that had descended within a major tropopause fold beneath the upper-level jet axis. Isentropic analysis showed that, relative to the moving PV maximum, dry high-PV air in the fold descended behind the PV maximum and ascended ahead of it, immediately behind and above the comma cloud. The PV maximum associated with the fold may have been responsible for the observed overrunning of low -θ_w air and the eventual production of an overall region of potential instability and convective overturning, as proposed by Griffiths et al (2000).

The WV imagery perspective

The PV maximum was associated with a well defined dark zone in the WV imagery which had the form of a 'dry eye' (Weldon & Holmes 1991) due to the descent of a compact region of stratospheric air. The 'dry eye' in the WV imagery formed over a 12-hour period as it approached the British Isles during which time the tropopause fold was extending downwards.

The cloud imagery perspective

The infrared satellite imagery showed the comma cloud as a cyclonically curved feature, over 1000 km long, wrapping around the leading edge of the jet streak and PV maximum. The cloud was capped along its full length by the tropopause fold/frontal zone and tops rose from near 3km along the tail of the comma cloud to 7 to 8 km over part of the head. Only the head was visible in the WV imagery because the tail was obscured by upper tropospheric moisture within the warm air of the upper-level jet. Striations were seen in the cloud tops in the WV and IR imagery and were especially clear in the visible. Careful enhancement of the visible images showed a whole series of mesoscale cloud bands whose integrity was confirmed by their correspondence to radar-detected rainbands. The individual mesoscale cloud bands tended to be shaped like open waves and the IR imagery showed that their tops ascended from low levels in their trailing cold frontal parts to higher levels in their warm frontal regions

The radar rainfall network perspective

The series of mesoscale rainbands was resolved clearly in the radar network pictures. Fifteen curved bands were observed, typically 70 km apart. Each was tracked for several hours. Inferred rainfall intensities over 5-km squares in excess of 8 mm h^{-1} were common along the axes of these bands, with peak 5-km values over 32 mm h^{-1}. Towards the tail of the comma cloud, the cold-frontal part of each rainband was elongated and displayed a shallow ana-cold frontal circulation. Closer to the head of the comma cloud, the precipitation along the cold-frontal part of each mesoscale band was suppressed by strongly overrunning dry air, i.e. kata cold-front circulation. The ana and kata circulations were deduced from both Doppler radar and mesoscale model diagnostics.

The Chilbolton Doppler radar perspective

Volume scans from this radar through one of the mesoscale rainbands revealed the classical ana-cold frontal structure of the trailing cold-frontal portion, with line convection giving a narrow cold-frontal rainband followed by a region of shallow rearward-sloping ascent. Analysis of the radar bright band, best seen in the linear depolarisation ratio, showed an abrupt drop in the θ_w of up to 3°C near the surface at the line convection. However, although the rainband was in a weakly cold-frontal region, the θ_w recovered to within a degree of the prefrontal temperature some 20 km behind, indicating that the magnitude of the temperature drop at the line convection was mainly due to local descent of low $-\theta_w$ air plus evaporation and melting-induced cooling. In most cold-frontal occurrences of line convection that we have observed in the UK, the line convection is shallow (typically 3km deep); however, in this case, the top of the line convection, though 3km or less in the trailing part of the line, rose to as high as 6 to 7 km near the northern end. This was probably due to the strong overrunning of low $-\theta_w$ air aloft as shown by the mesoscale model. In advance of this, where the rainband curved back towards the southeast, the radar showed that there was widespread rather uniform stratiform precipitation. The analysis of bright-band height showed that this was associated with a weak warm-frontal zone.

The mesoscale model perspective in relation to the radar-observed rainbands.

Comparison with various observations revealed that the model reproduced the overall features of the comma-cloud system quite well. We draw attention to some specific shortcomings later. An important contribution of the model was to clarify the interaction between the dry air seen in the WV imagery and the tongue of moist air travelling along the axis of the comma cloud. The dominant behaviour was for the dry air to overrun the moist air particularly above 3km (700 mb). The dry air was characterised by relatively low θ_w and it led to extensive potential instability. Some of the dry low $-\theta_w$ air also undercut the moist air and penetrated to the surface immediately behind the line convection; this convection fed a shallow slantwise ana-cold frontal circulation which intruded back into the predominantly overrunning low $-\theta_w$ air.

The model showed that the low $-\theta_w$ air above 700 mb tended to overrun the moist air not along a uniform front but, rather, as a series of mesoscale intrusions that became elongated with time. Some of the intrusions related well to observed dry intrusions associated with individual mesoscale bands. One well marked dry intrusion was associated with a relatively large gap in the precipitation that followed the rainband observed by the Chilbolton radar. But, for the most part, these features were on the borderline of the capability of the model to resolve them.

The Aberystwyth MST radar perspective in combination with the mesoscale model.

The MST radar was useful in depicting the laminated structure of the atmosphere and the airflow patterns in and around the jet streak exit, including the underlying region of dry air that interacted with the comma cloud. The good agreement with the mesoscale model gave confidence in the use of the latter. Combining the MST radar data with output from the model and with 6-hourly radiosondes, it was possible to show with some confidence that very dry air and very high PV (5 to 6 PVU according to the model) descended in the tropopause fold to below 6 km just behind the comma cloud, effectively at the focus of the comma cloud system. The centre of the localized PV maximum when it passed over Aberystwyth was just 2km above the tops of the air rising slantwise in the trailing parts of the cloud bands and is presumed to have been playing a dynamically active role. The dry low $-\theta_w$ air that was intruding into the moist comma-cloud air was tropospheric air from just beneath the tropopause fold near its local PV-maximum. The rising air within the comma cloud itself ascended into the tropopause-break region, the top of the leading part of the cloud system forming its own local tropopause.

The MST radar revealed some significant fine-scale structure not resolved by the mesoscale model. Above the upper-level jet, just in the stratosphere, there was a secondary layer of high winds which, in view of the 2km vertical wavelength and perturbation wind vector rotating clockwise with height, was evidently an inertia-gravity wave. A similar layer, but with perturbation wind vector rotating anticlockwise, was observed just beneath, in the upper troposphere. Laminations in velocity and stability were also observed farther below the jet. Some of these were within the very dry air of the tropopause fold/frontal zone and some weaker ones were just below in the dry low $-\theta_w$ tropospheric air that was intruding into the comma cloud. These same perturbations were also resolved by the operational UHF wind

profiler radar at Camborne where they extended right into the region of the rainbands. They may be related to the tendency of the mesoscale model to generate fingers of more rapidly advancing dry air. These fingers were within the cyclonic flow induced just below the PV maximum and we speculate that they may have been the cause of the mesoscale bandedness within the comma cloud. Possibly the multiplicity of these fingers was related to the multiplicity of laminations created by the inertia-gravity waves.

8. The capability of the mesoscale model to resolve the mesoscale substructure

We have used the MST radar data to show that the operational UK Met Office mesoscale model reproduced the broad pattern of horizontal wind well (Fig.14(a)). We have also found (not shown here) that the predicted rainfall distributions fit well with those observed by the weather radar network, albeit with a 60km displacement error. The model was also quite good in predicting the rather high intensity of the rainfall, giving patches of 10 mm h^{-1} rainfall averaged over 17km compared with the observed patches in excess of 32 mm h^{-1} averaged over 5km. The model did not, however, show much in the way of realistic mesoscale rainband organisation; nor did it appear to get the location of rain cores right in anything other than a statistical sense. Severe weather events, such as (brief) torrential downpours, lightning and a (small) tornado, occurred on this occasion in association with the more intense segments of line convection. The need to develop techniques for the site-specific very-short-range prediction of such events makes it desirable if possible to extend the capability of the model to represent such events.

The results of this study provide us with grounds for limited optimism that the mesoscale model can be developed to handle these severe local events. Our optimism is based upon the following findings:

1) The model appeared to reproduce the main mesoscale driver, the tropopause fold and associated PV maximum, well. This is presumably because the global model which provides the boundary forcing for the mesoscale model represented the large-scale synoptic evolution that led to the fold.
2) The model represented not only the broad (meso-alpha) region of overrunning dry low -θ_w air but also reproduced some of the meso-beta scale fingers of dry air that were associated with individual mesoscale rainbands. It resolved the largest finger

(lateral scale ~100km) associated with Rainband 7 but had difficulty with the other smaller rainbands (lateral scale ~50 km).

3) The model correctly represented a region of rearward-sloping ascent (ana-cold frontal circulation) in the correct location within the overall region of overrunning (kata-type circulation). This is encouraging because observational studies indicate that intense line convection often occurs in association with ana-cold frontal circulations.

The more obvious shortcomings of the model are:

1) The present model did not resolve the line convection itself since the width of the convective updraughts is 3km or less, much less than the model grid spacing.

2) Whilst the model resolved the largest of the dry fingers (lateral scale ~ 100 km) associated with Rainband 7, it had difficulty with the dry fingers associated with the other smaller rainbands (lateral scale ~50 km).

3) Although the model's representation of the horizontal winds was shown to be generally quite good, it failed to represent the large-amplitude inertia-gravity waves near tropopause level from 15 to 23 UTC as revealed by the darkly shaded layer of maximum observed winds between 11 and 12 km in Fig.14(a).

An increase in model resolution may improve the capability to represent the smaller features. The dry fingers were associated with individual mesoscale rainbands and we have speculated that these fingers were associated with some kind of small-scale wave disturbances originating from the vicinity of the jet streak exit and PV maximum. The mechanism responsible for the disturbances may be inertia-gravity wave activity. It is possible that increasing the model resolution will enable it to represent the existence of such features within a general mesoscale region but not their exact location. The fact that the larger finger associated with Rainband 7 was predicted in the correct location may indicate the beneficial influence of observational data assimilated into the model.

9. Conclusions

Local severe-weather events often occur in association with convection organised on the mesoscale within larger-scale weather systems. It is common for this to occur within cold-air troughs, themselves mesoscale in size but nevertheless containing much smaller mesoscale substructures. Observing, understanding and predicting such events is difficult because of the multi-scale nature of such events. In this paper we have carefully investigated one such occasion: a vigorous comma cloud occurring in the cold air in the exit region of an upper-level jet streak. In this observational study we have synthesised data from many sources, including routine synoptic, satellite and radar data, and information from specialised research radars. We have also used output from an operational mesoscale model both to supplement the observations and to evaluate its capability to represent features of very small scale.

At first sight the distribution of precipitation and embedded convection appears highly complex, but detailed scrutiny has shown it to be associated with a series of mesoscale rainbands each resembling a mesoscale open wave. A key ingredient of the mesoscale organization is the overrunning of dry air with low wet-bulb potential temperature. This occurs in the form of mesoscale fingers, possibly one per rainband although the observations are inadequate to confirm this. Wind fluctuations in the form of a series of wave fronts were also detected within the dry air just above and behind the rainbands, extending from the region of very dry stratospheric air within the deeply penetrating tropopause fold, into the small region of fairly dry low $-\theta_w$ tropospheric air sandwiched between the fold and the rainbands. It is speculated that the occurrence of the multiple convective rainbands was related to the series of wave fronts or wind pulsations originating in the region of the jet exit and PV maximum. These pulsations were only weakly resolved by the observations but may have been related to large-amplitude inertia-gravity waves detected closer to the upper-level jet core.

The operational mesoscale model performed well in reproducing the overall region of precipitation with embedded heavy convective rainfall. Because of the likely importance of the PV anomaly associated with the tropopause fold and the role of the overrunning fingers of low $-\theta_w$ air in organizing the convective precipitation, it is encouraging that it appeared to represent these to some extent. While some of the mesoscale features were just large enough for the associated fingers to be resolved, others were not. It is suggested that

improving the resolution of the model will increase its ability to represent these important features.

Acknowledgements

The Joint Centre for Mesoscale Meteorology is supported by the Meteorological Office and the Department of Meteorology, University of Reading. The research was undertaken under the auspices of the Universities Weather Research Network (UWERN) funded by the Natural Environment Research Council. We are grateful to the Meteorological Office for giving access to radar, satellite and Unified Model data and for providing support for wind profiler research, to Tim Oakley for provision of high-resolution wind-profiler data from Camborne, to staff from the Rutherford Appleton Laboratory for provision of data from the Chilbolton Doppler radar, to Ken Slater and the British Atmospheric Data Centre for high-resolution data from the MST radar at Aberystwyth, and to Wyn Jones, Gavin Winter and Danny Chapman, for assistance in data processing.

References

Astin, I. and Thomas, L. 1991 'The accuracy and precision of radar wind measurements'. Pp 15-20 in Proceedings of the fifth workshop on technical and scientific aspects of MST radar. Ed. B. Edwards. SCOSTEP, U. of Illinois, Urbana, USA.

Browning, K.A. 1990 Organization of clouds and precipitation in extratropical cyclones, In 'Extratropical cyclones', Eds. C.W. Newton and E.O. Holopainen, Am.Meteorol.Soc., pp129-153.

Browning, K.A. and Golding, B.W. 1995 Mesoscale aspects of a dry intrusion within a vigorous cyclone. *Q.J.R.Meteorol.Soc.*, **121,** 463-493.

Businger, S. and Hobbs, P.V. 1987 Mesoscale structures of two comma cloud systems over the Pacific Ocean. *Mon.Weather Rev.*, **115**, 1908-1928.

Businger, S. and Reed, R.J. 1989 Cyclogenesis in cold air masses. *Weather and Forecasting,* **4,** 133-156.

Businger, S. and Walter, B, 1988 Comma cloud development and associated rapid cyclogenesis over the Gulf of Alaska: a case study using aircraft and operational data. *Mon.Weather Rev,* **116**, 1103-1123.

Carlson, T. 1980 Airflow through midlatitude cyclones and the comma cloud pattern. *Mon.Weather Rev.***108**, 1498-1509.

Cullen, M.J.P., 1993, The unified forecast/climate model, *Meteorol.Mag.*, **122**, 89-94.

Goddard, J.W.F., Eastment, J.D., and Thurai, M. 1994 The Chilbolton advanced meteorological radar: a tool for multidisciplinary research. *Electronics and Communications Engineering,* **6**, 77-86.

Griffiths, M., Thorpe A.J. and Browning, K.A. 1999 Convective destabilization by a tropopause fold diagnozed using potential vorticity inversion. *Q.J.R.Meteorol.Soc.,* **125**, In press.

Harrold, T.W. and Browning, K.A, 1969 The polar low as a baroclinic disturbance. *Q.J.R.Meteorol.Soc.,* **95,** 710-723.

Heinemann, G. and Claud, C. 1997 Report of a workshop on "Theoretical and observational studies of polar lows" of the European Geophysical Society Polar Lows Working Group. *Bull.Am.Meteorol.Soc.,***78**, 2643-2658.

Houze, R.A.,Jr., 1981 Structures of atmospheric precipitation systems – a global survey, *Radio Science*, **16**, 671-689.

Locatelli, J.D, Hobbs, P.V. and Werth, J.A. 1982 Mesoscale structures of vortices in polar air streams. *Mon.Weather Rev.* **110,** 1417-1433.

Lorenc, A.C., Bell, R.S. and Macpherson, B., 1991. The Meteorological Office analysis correction data assimilation scheme. *Q.J.R.Meteorol.Soc.,* **117,** 59-89.

Macpherson, B., Wright, B.J., hand, W.H. and Maycock, A.J., 1996, The impact of MOPS moisture data in the UK Meteorological Office Mesoscale Data Assimilation Scheme, *Mon.Weather Rev.* **124,** 1746-1766.

Mullen, S.L. 1979 An investigation of small synoptic-scale cyclones in polar airstreams. *Mon.Weather Rev,* **107,** 1636-1647.

Panagi, P.M., and Dicks E.M., 1997. Met. Office Unified Model data, diagnostics, graphics programs and other observational data available from JCMM through the aegis of the Universities Weather Research Network, UWERN, JCMM Internal report 69 + supplement.

Reed, R.J. 1979 Cyclogenesis in polar air streams. *Mon.Weather Rev.,* **107**, 38-52.

Slater, K., Stevens, A.D., Pearmain, S.A.M., Eccles, D., Hall, A.J., Bennett, R.G.T., France, L., Roberts, G., Olewicz, Z.K., and Thomas, L. 1991 'Overview of the MST radar system at Aberystwyth'. Pp 479-482 in Proceedings of the fifth workshop on technical and scientific aspects of MST radar. Ed. B. Edwards. SCOSTEP, U. of Illinois, Urbana, USA.

Thomas, L., Prichard, I.T., and Astin, I. 1992 Radar observations of an inertia-gravity wave in the troposphere and lower stratosphere, *Ann.Geophys.,* **10**, 690-697.

Uccellini, L.W. and Johnson, D.R. 1979 The coupling of upper-and lower-tropospheric jet streaks and implications for the development of severe convective storms. *Mon.Weather Rev,***107**, 682-703.

Vaughan, G., Howells, A. and Price, J.D. 1995 Use of MST radars to probe the mesoscale structure of the tropopause. *Tellus,* **47A,** 759-765.

Weldon, R.B. and Holmes, S.J. 1991 Water vapour imagery, interpretation and applications to weather analysis and forecasting. *NOAA Tech.Report NESDIS 57,* 213pp.

Yang, M.J. and Houze Jr, R.A. 1995 Sensitivity of squall-line rear inflow to ice microphysics and environmental humidity. *Mon.Weather Rev.,* **123,** 3175-3193.

Zick, C., 1983 Method and results of an analysis of comma cloud developments by means of vorticity fields from upper-tropospheric satellite wind data. *Meteorol.Rdsch.*, **36**, 69-84.

FIGURE LEGENDS

Fig. 1 Schematic diagram showing typical relationship of comma cloud to a major frontal cyclone and upper-level jet (from Zick 1983).

Fig. 2 Meteosat water vapour image for 1230 UTC, 26 January1999, showing the comma cloud over England and Wales ahead of a dry intrusion (dark zone) over the Irish Sea.

Fig. 3 Mesoscale model analyses at 12 UTC, 26 January 1999. (a) MSL pressure. The bold line represents the trough associated with the comma cloud; one hour later a closed low formed at 54° N, 2½° W. The associated tongue of warm air approaching from the southwest is shown by the dashed isopleth for 900mb θ_w = 281 K. (b) Upper- and lower-level jets. The upper-level jet is represented by the 60 ms^{-1} isotach at 300 mb and the low-level jet by the 22 ms^{-1} isotach at 800 mb. The bold arrows represent the flows within these jets and the thin arrow shows the track of the potential vorticity anomaly in Fig. 4.

Fig. 4 Mesoscale model analysis for the 295 K dry isentropic surface at 12 UTC, 26 January 1999. Thin contours represent geopotential height at 500 m intervals; shading represents potential vorticity on a scale from 0 to 6 PV units (dark for high PV except for the small white spot for the PV maximum over Northern Ireland where PV>6); arrows represent winds relative to the motion of the PV maximum; thick contours represent vertical velocity, with a main region of ascent (> 5 cm s^{-1}) southwest of the PV maximum and descent (< -5 cm s^{-1}) northwest of it.

Fig. 5 Weather radar network pictures for (a) 1515 and (b) 1600 UTC, 26 January 1999. Colours represent mean rainfall rate in 5 km squares: blue < 0.5, olive 0.5 to 1, green 1 to 2, yellow 2 to 4, orange 4 to 8, red 8 to 16, maroon 16 to 32, green 32 to 64 mm h^{-1}. Numbered thin lines highlight individual rainbands.

Fig. 6 Meteosat images for 1400 UTC, 26 January 1999: (a) visible, (b) infrared. Colour scales are chosen to highlight key features discussed in text. In (a) blue (with white cores) corresponds to the brightest cloud whilst light colours correspond to dark regions. In (b) the colours represent cloud-top brightness temperatures as follows:

yellow <230, sepia 230 to 236, orange 236 to 245, red 245 to 257, maroon 257 to 264 K. Areas warmer than 264 K are shown blue.

Fig. 7 Analysis of Rainband 7 at 1622 UTC (± 11 mins) on 26 January 1999, based on a set of RHI scans by the Chilbolton radar at 20° azimuth intervals. Thick contours represent the extent of echo (> -10 dBz) at heights of ½ km (dashed), 1½, 4 and 6 km (solid lines). Patches of echo behind the main rainband have been omitted for simplicity. Thin contours represent wet-bulb potential temperature, θ_w = 2,3, 4 and 5° at bright-band level (between 400 m and 1 km). The chain of digits represents the height (in km) of the 40 dBz echo due to line convection along the surface cold front. Two fine arrows schematically represent perturbation flows at low levels responsible for the curvature of the tongue of warm air on one side of the intense line convection and the evaporationally-induced indentation of the low-level (½ km) echo on the other.

Fig. 8 Range-height (RHI) scans from the Chilbolton radar at 1624 UTC (± 4 min), 26 January 1999, showing reflectivity (dBz) along azimuths (a) 090°, (b) 130° and (c) 230°, and (d) vertical shear of the Doppler velocity along azimuth 230°.

Fig. 9 Summary diagram showing the multiple rainbands (numbered curves) at 1600 UTC, 26 January 1999, stacked along the axis of the 850 mb θ_w-maximum (dotted curve WW) and situated ahead of the 300 mb jet core (isotachs at 65 and 70 m s^{-1}). Rainbands shown dashed correspond to the extrapolated position of bands that decayed shortly before 1600 UTC. 'A' marks the location of the MST radar at Aberystwyth and the solid and open arrows, respectively, indicate the velocities with which the individual rainbands and the upper-level jet advected overhead.

Fig. 10 Time-height section of (a) wind strength (m s^{-1}), (b) westerly wind component (m s^{-1}) and (c) radar echo power (dBz), obtained with the MST radar at Aberystwyth (A) on 26 January1999. Wind measurements in (a) and (b) are 9-minute running averages of data obtained every 1.5 mins; noisy signals that appeared at 3 times, and are believed to have been caused by convection, have been eliminated before averaging. The overplotted solid and dotted lines highlight axes of local wind

maxima as discussed in the text, and the passage of convection associated with Rainband 5 is indicated in (b) by the vertical arrow. Radar power measurements in (c) are plotted every 1.5 min to reveal fine structure; the overplotted solid and dotted lines highlight layers of high power as discussed in the text. The Ts and Xs in (c) correspond to the tropopause and upper and lower edges of the tropopause fold as identified in Fig.11.

Fig.11 Tephigrams for radiosondes released from Aberporth (near Aberystwyth) at (a) 12 UTC and (b) 17 UTC, 26 January 1999. Solid lines, temperature. Dashed lines, dew point. Labels T and X correspond to those plotted in Fig.10(c).

Fig.12 Hodographs of perturbation velocity from selected heights (a) above and (b) below the tropopause, derived from the 15-min averaged MST radar sounding at Aberystwyth centred at 18 UTC, 26 January 1999. The lowest height in each case is marked by a solid square and successive heights are at 150m intervals. The direction of rotation with increasing height is indicated by arrows.

Fig.13 Time-height section of radar echo power (dBz) obtained with the wind profiling radar at Camborne on 26 January 1999. Dark grey columnar echoes are from precipitation particles associated with the passage of successive convective rainbands. Pale grey echo layers are from clear-air refractive-index inhomogeneities. See text for explanation of the dotted and scalloped lines.

Fig.14 Time-height sections over Aberystwyth of (a) westerly wind component, (b) relative humidity with respect to ice, and (c) potential vorticity, obtained from the mesoscale model on 26 January 1999. See text for details of derivation. (a) shows model-derived contours for 25 and 35 m s^{-1} superimposed on hourly-smoothed MST radar values given as a simplified grey-scale with steps also at 25 and 35 ms^{-1}. (b) and (c) show the model-derived RH and PV as grey scales, with steps at intervals of 10% and 1 PV unit, respectively. Superimposed on both (b) and (c) are features copied from the MST radar section in Fig.10(c).

Fig.15 Sections through the comma cloud system obtained from the 12 UTC forecast run of the mesoscale model on 26 January 1999. (a) and (b) show relative humidity (5% intervals) at 16 UTC, at 800 and 600 mb, respectively; areas with RH≥100% are shaded. The bold lines in (a) shows the rear edge of saturated air at 700 mb, the dark

shading just ahead of it indicating the extent to which it is behind that at 800 mb. The dotted line in (a) shows the position of the observed line convection associated with Rainband 7, and the X marks the location of the Chilbolton radar. (c) shows successive hourly positions, from 12 to 17 UTC, of the rear edge of saturated air at 600 mb, the development of individual fingers of dry air being highlighted by arrows. (d) shows relative humidity (5% intervals) at 16 UTC within the vertical section along AA' in (a); key features are labelled and saturated regions are shaded. (e) shows the wet-bulb potential temperature (contours at 1K intervals) along the dashed curve BB' in (a); superimposed are potential vorticity (thick contour for PV=1 PV unit), the position of the 295K dry isentropic surface (dashed contour) and the extent of saturated air (shaded).

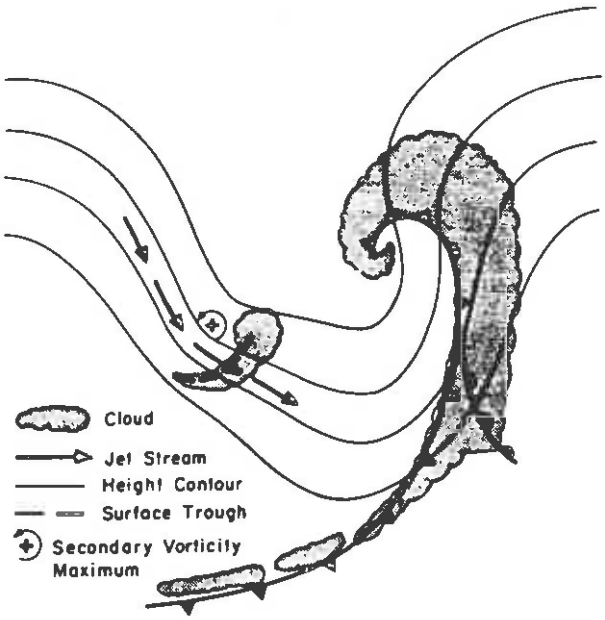
Cloud
Jet Stream
Height Contour
Surface Trough
Secondary Vorticity Maximum

Fig 1

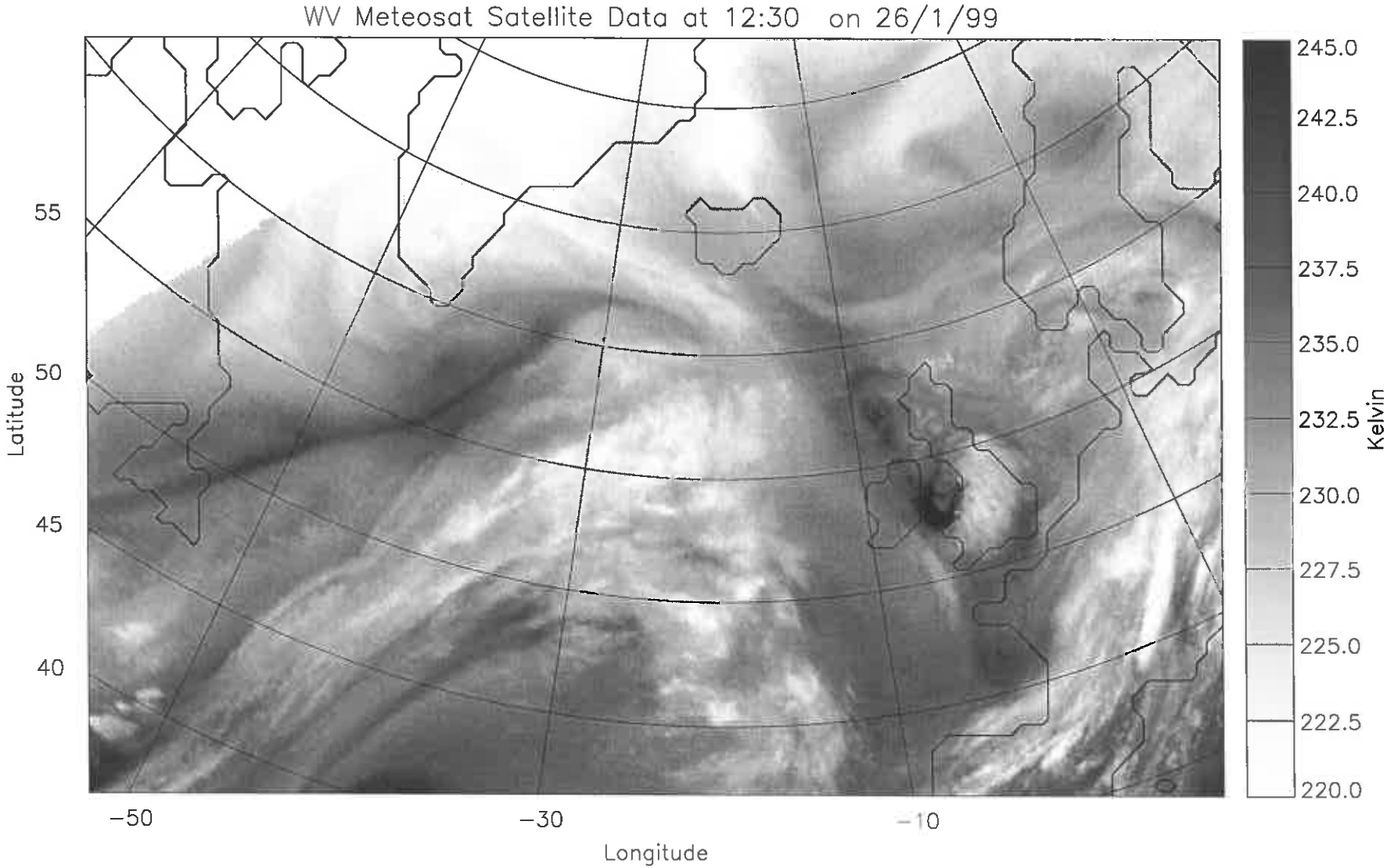
WV Meteosat Satellite Data at 12:30 on 26/1/99
Latitude
55
50
45
40
−50
−30
−10
Longitude
245.0
242.5
240.0
237.5
235.0
232.5
230.0
227.5
225.0
222.5
220.0
Kelvin

Fig. 2

not the original

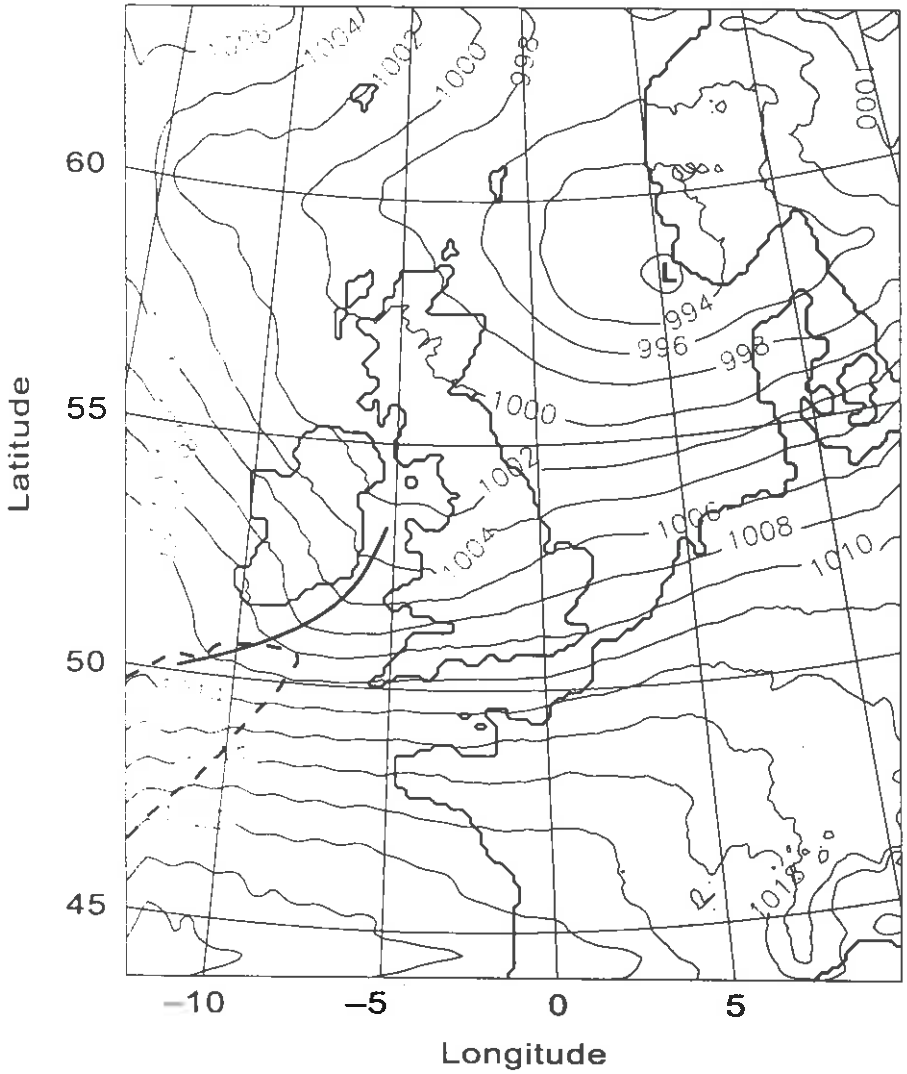

Fig 3a

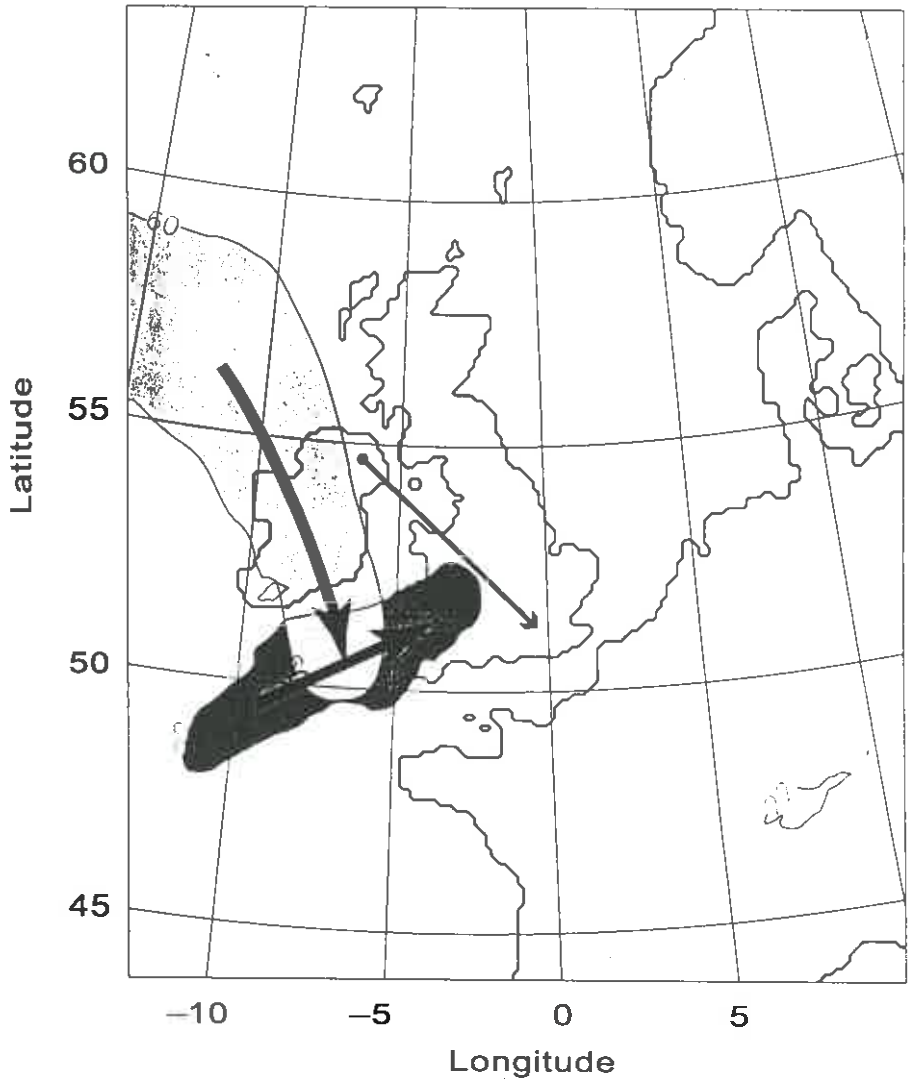

Fig 3b

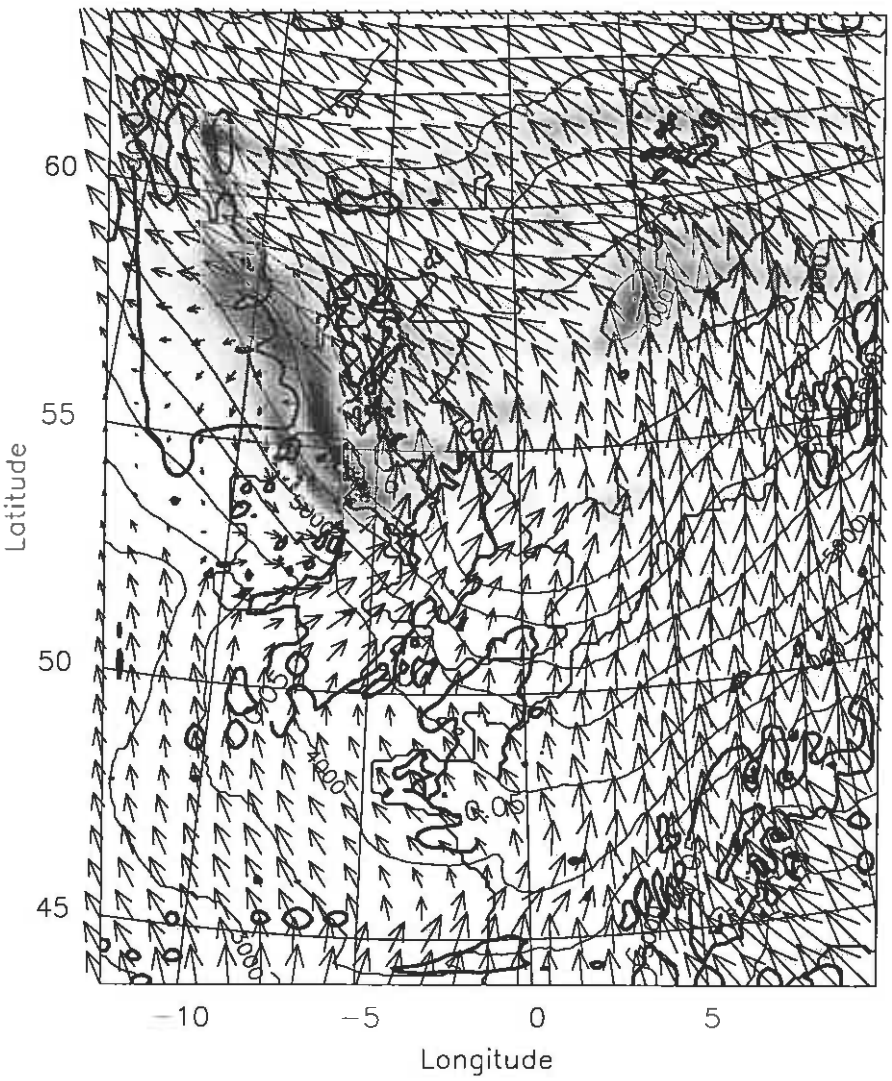

Fig. 4

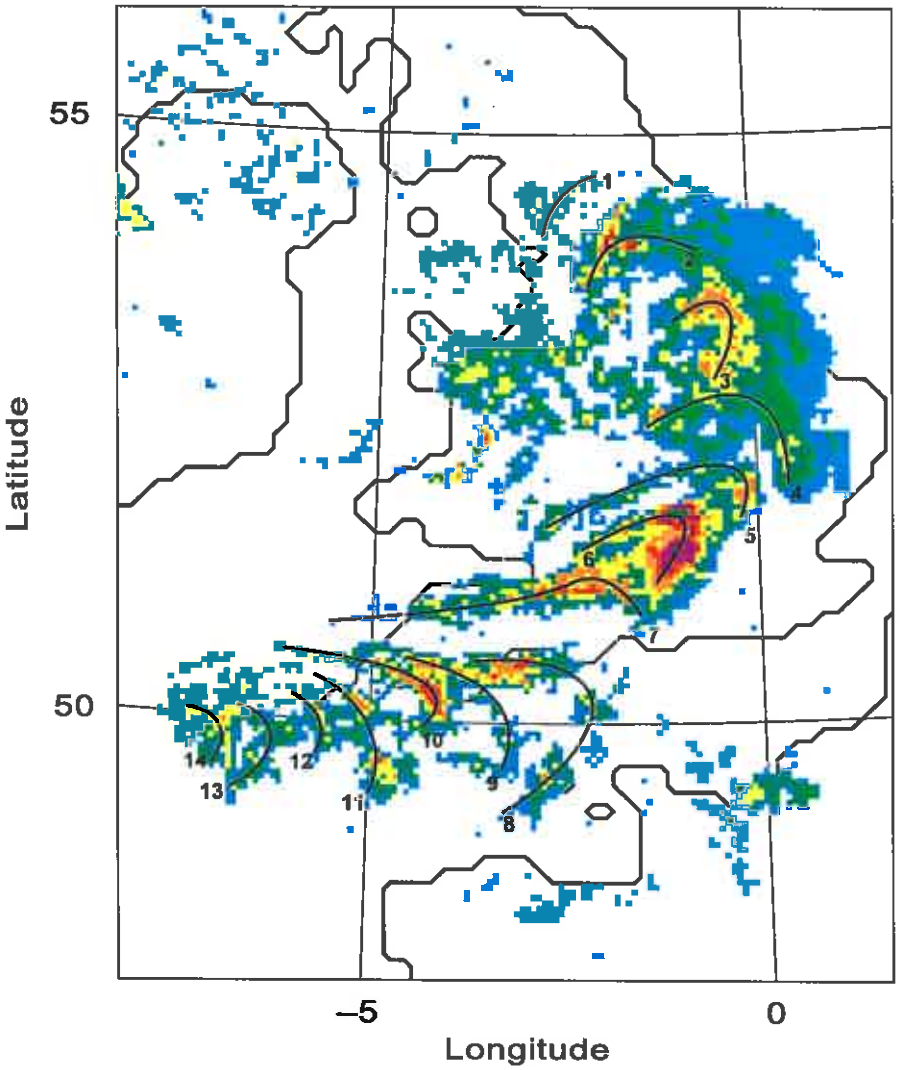
55
50
Latitude
−5
0
Longitude
1
2
3
4
5
6
7
8
9
10
11
12
13
14

Fig 5a

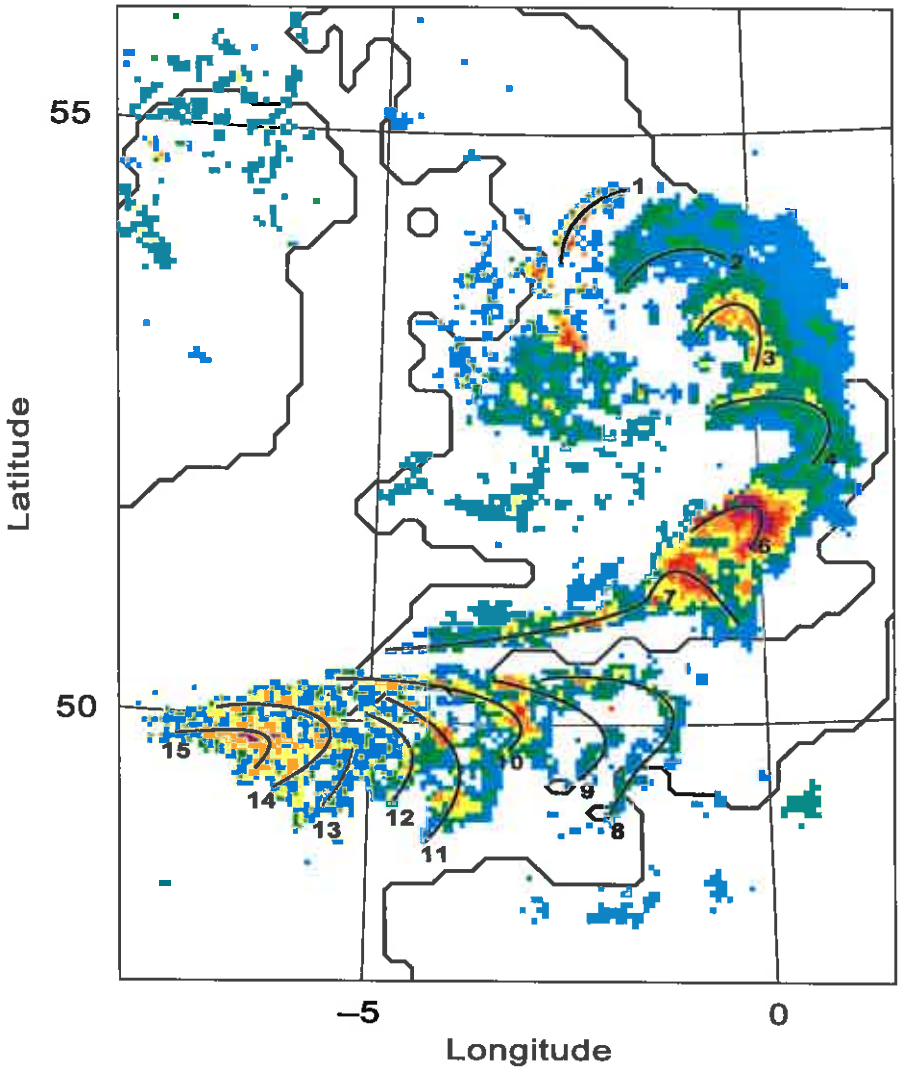
55
50
Latitude
−5
0
Longitude
1
2
3
4
5
6
7
8
9
10
11
12
13
14
15

Fig 5b

Fig 6(a)

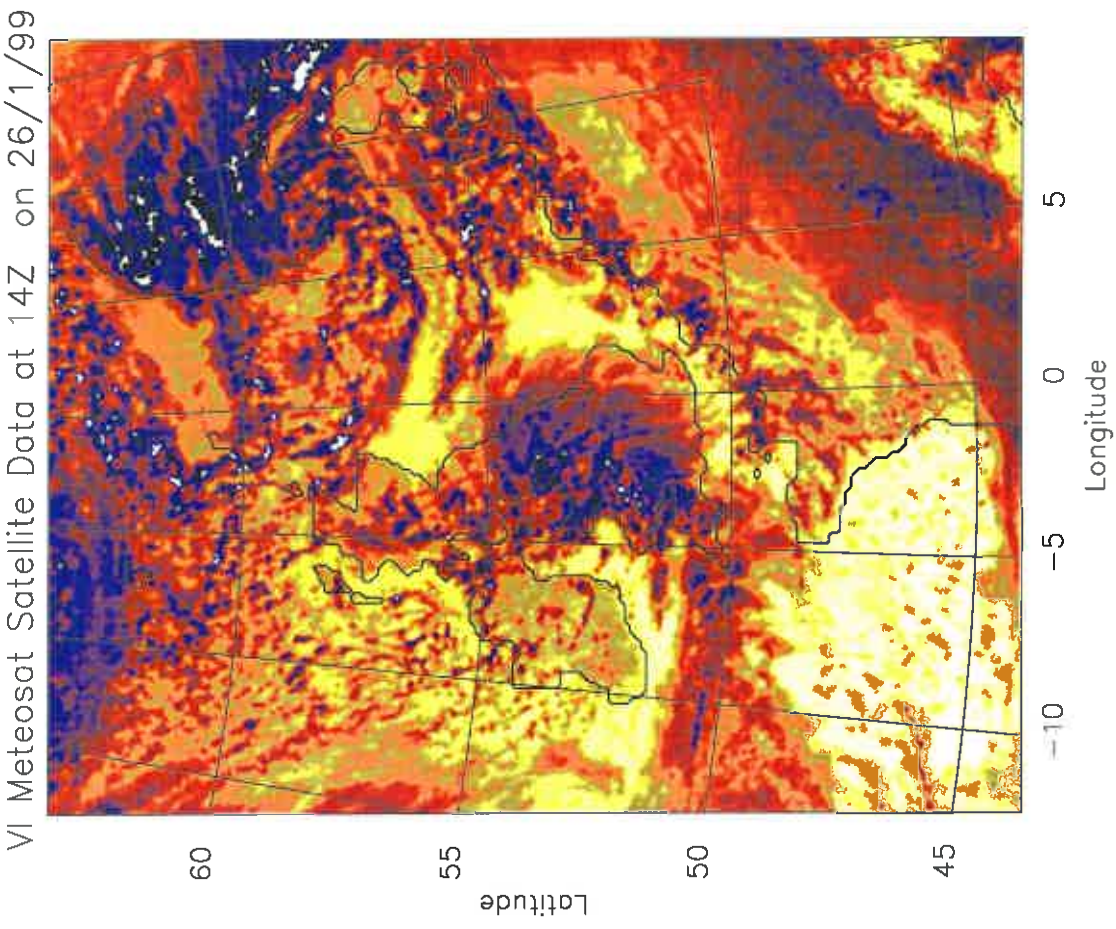
VI Meteosat Satellite Data at 14Z on 26/1/99
Latitude
60
55
50
45
-10
-5
0
5
Longitude

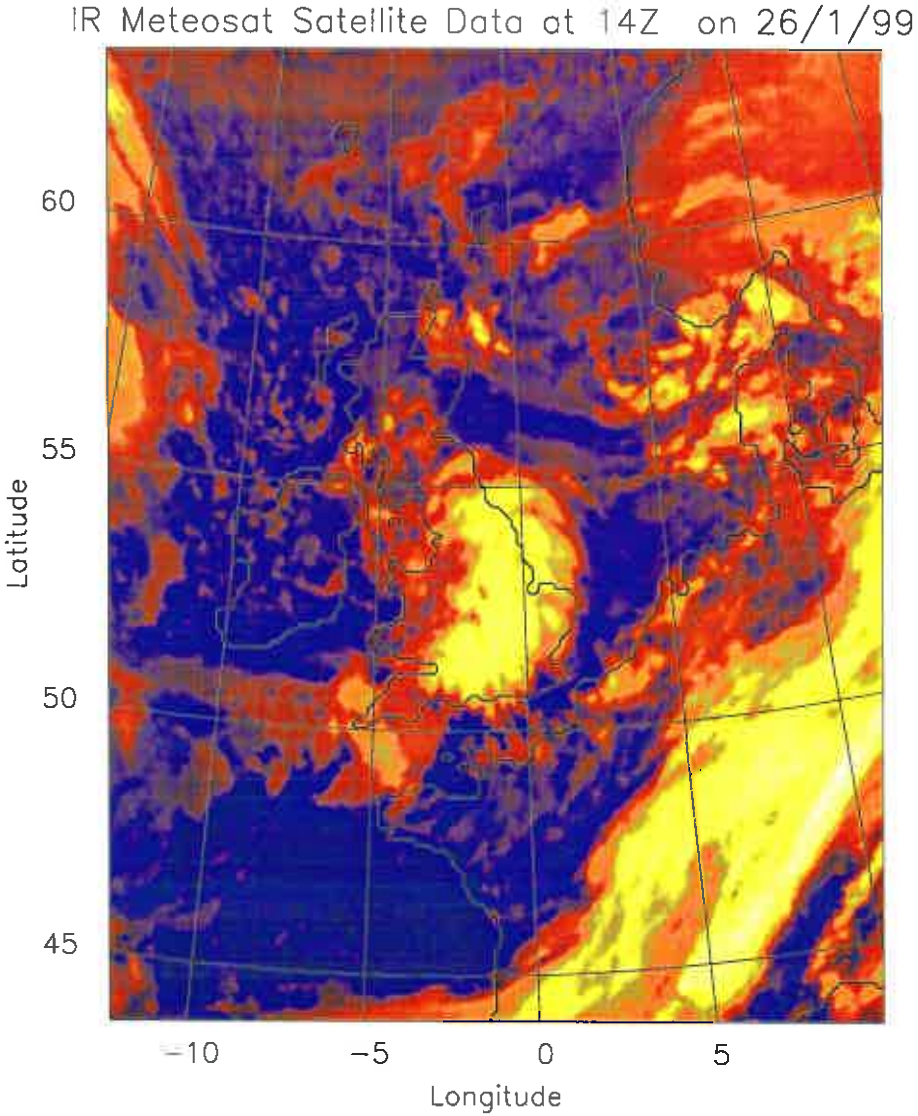
IR Meteosat Satellite Data at 14Z on 26/1/99
60
55
50
45
Latitude
−10
−5
0
5
Longitude

Fig 6(a)

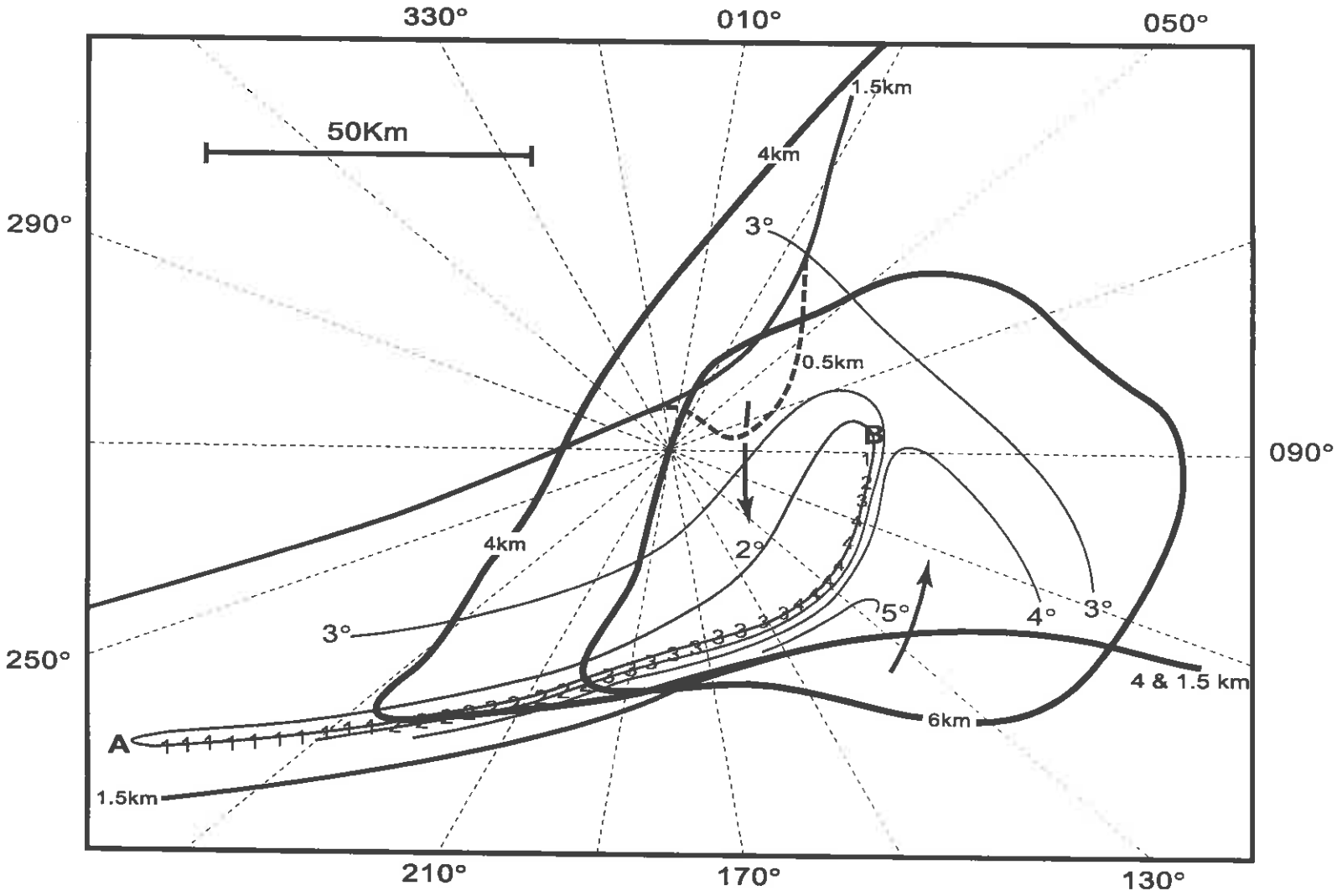
330°
010°
050°
290°
090°
250°
210°
170°
130°
50Km
1.5km
4km
3°
0.5km
4km
2°
3°
5°
4°
3°
4 & 1.5 km
6km
A
B
1.5km

Fig 7

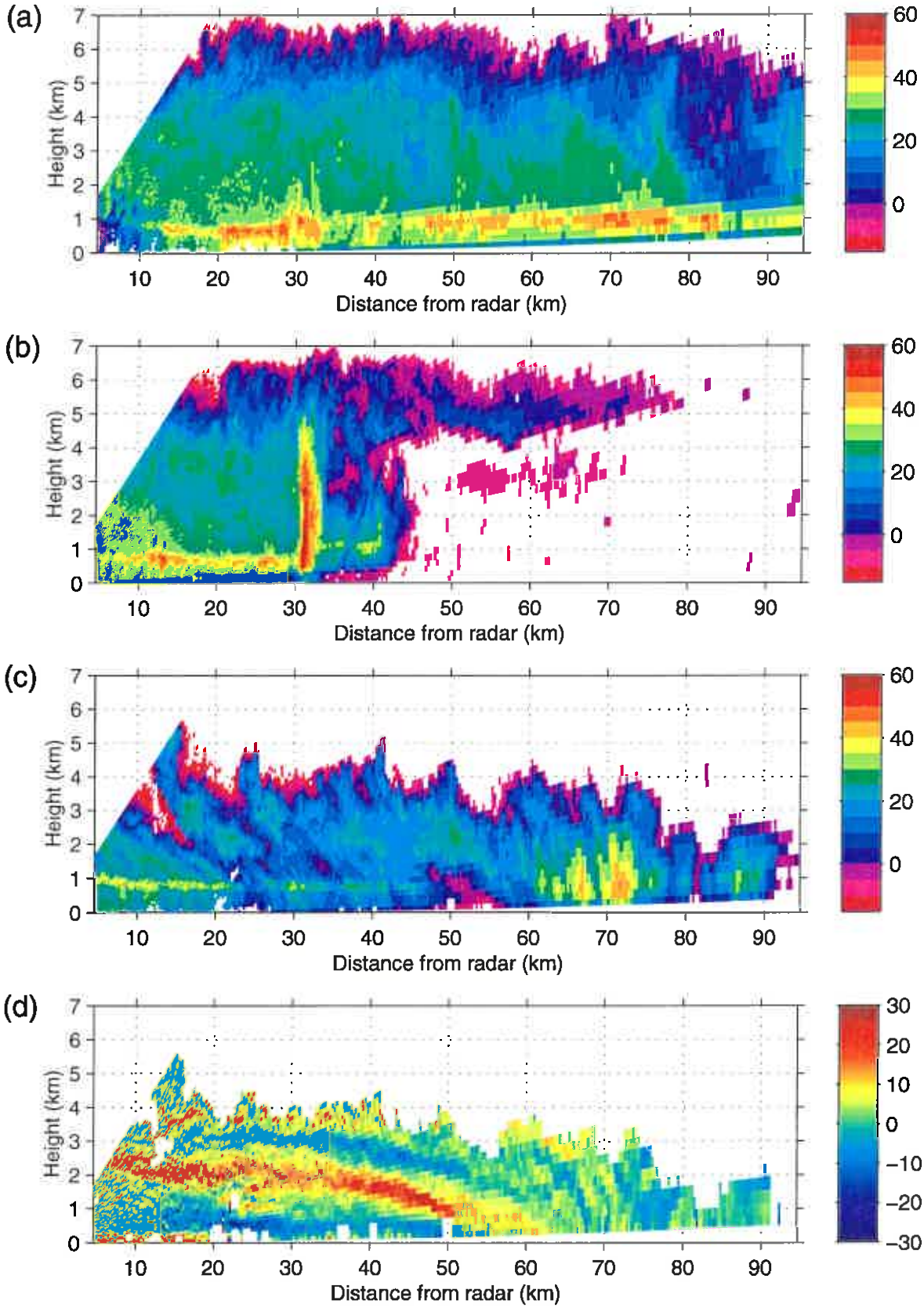
(a)
Height (km)
Distance from radar (km)
(b)
Height (km)
Distance from radar (km)
(c)
Height (km)
Distance from radar (km)
(d)
Height (km)
Distance from radar (km)

Fig. 8

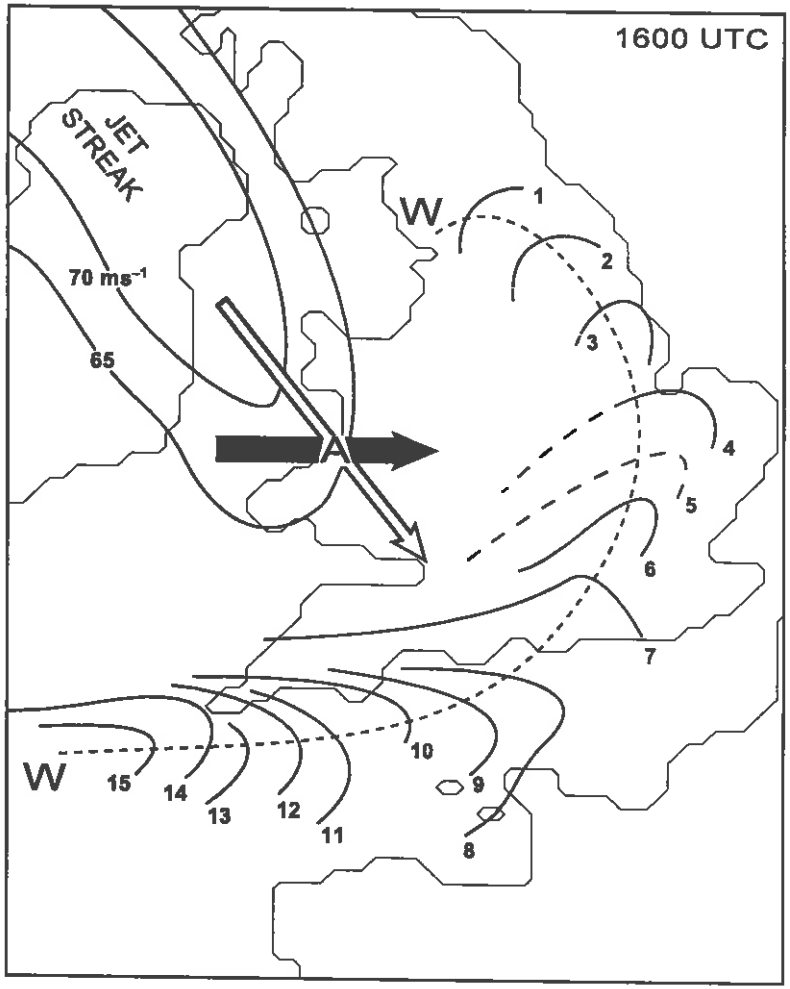

Fig 9

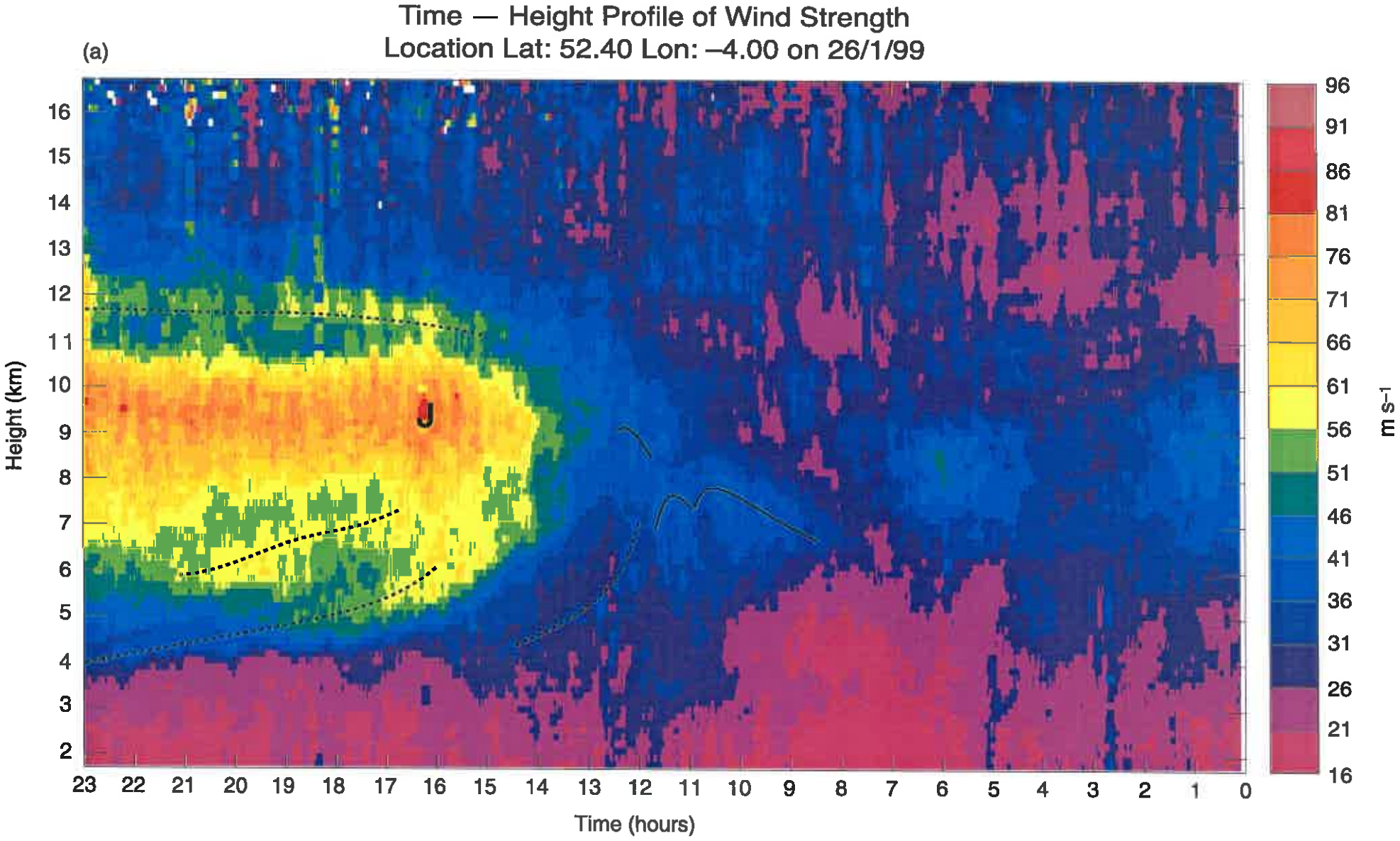
Time — Height Profile of Wind Strength
Location Lat: 52.40 Lon: –4.00 on 26/1/99
(a)
Height (km)
16
15
14
13
12
11
10
9
8
7
6
5
4
3
2
J
23 22 21 20 19 18 17 16 15 14 13 12 11 10 9 8 7 6 5 4 3 2 1 0
Time (hours)
96
91
86
81
76
71
66
61
56
51
46
41
36
31
26
21
16
m s⁻¹

Fig 10a

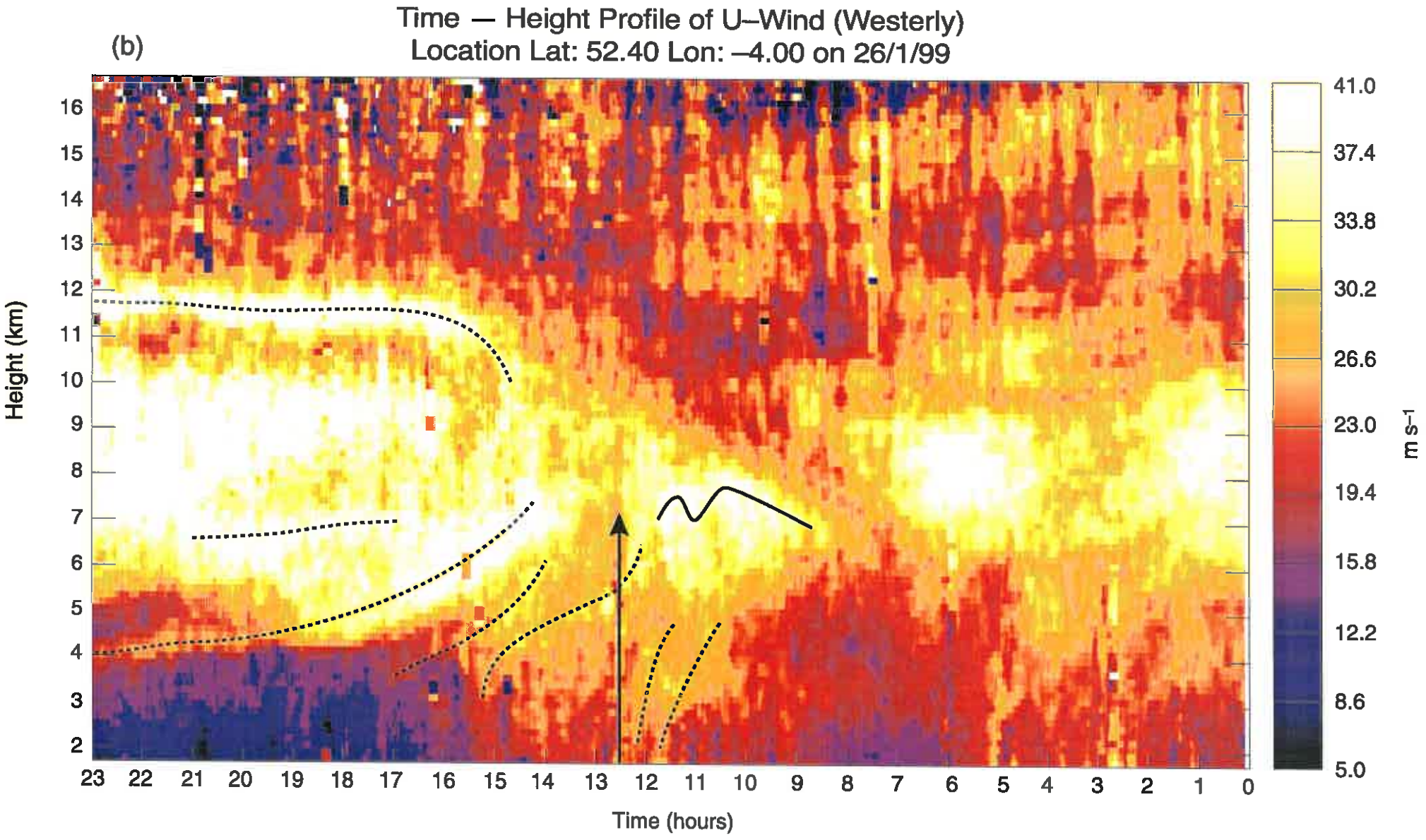
Time — Height Profile of U–Wind (Westerly)
Location Lat: 52.40 Lon: –4.00 on 26/1/99
(b)
Height (km)
16
15
14
13
12
11
10
9
8
7
6
5
4
3
2
23 22 21 20 19 18 17 16 15 14 13 12 11 10 9 8 7 6 5 4 3 2 1 0
Time (hours)
41.0
37.4
33.8
30.2
26.6
23.0
19.4
15.8
12.2
8.6
5.0
m s⁻¹

Fig 10b

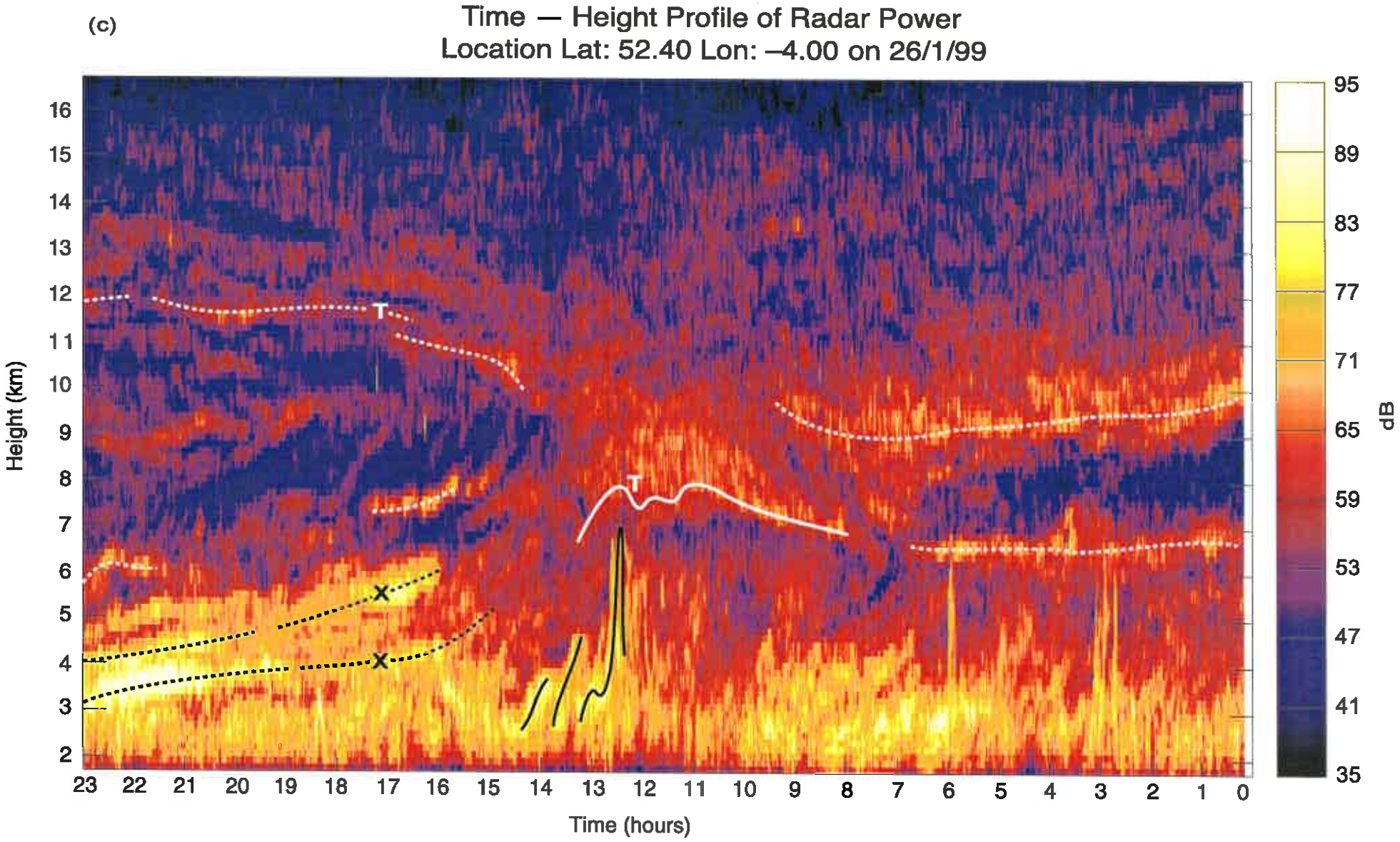
(c)
Time — Height Profile of Radar Power
Location Lat: 52.40 Lon: –4.00 on 26/1/99
Height (km)
16
15
14
13
12
11
10
9
8
7
6
5
4
3
2
T
T
X
X
23 22 21 20 19 18 17 16 15 14 13 12 11 10 9 8 7 6 5 4 3 2 1 0
Time (hours)
95
89
83
77
71
65
59
53
47
41
35
dB

Fig 10c

(a) Aberporth Radiosonde
26/01/99 12Z

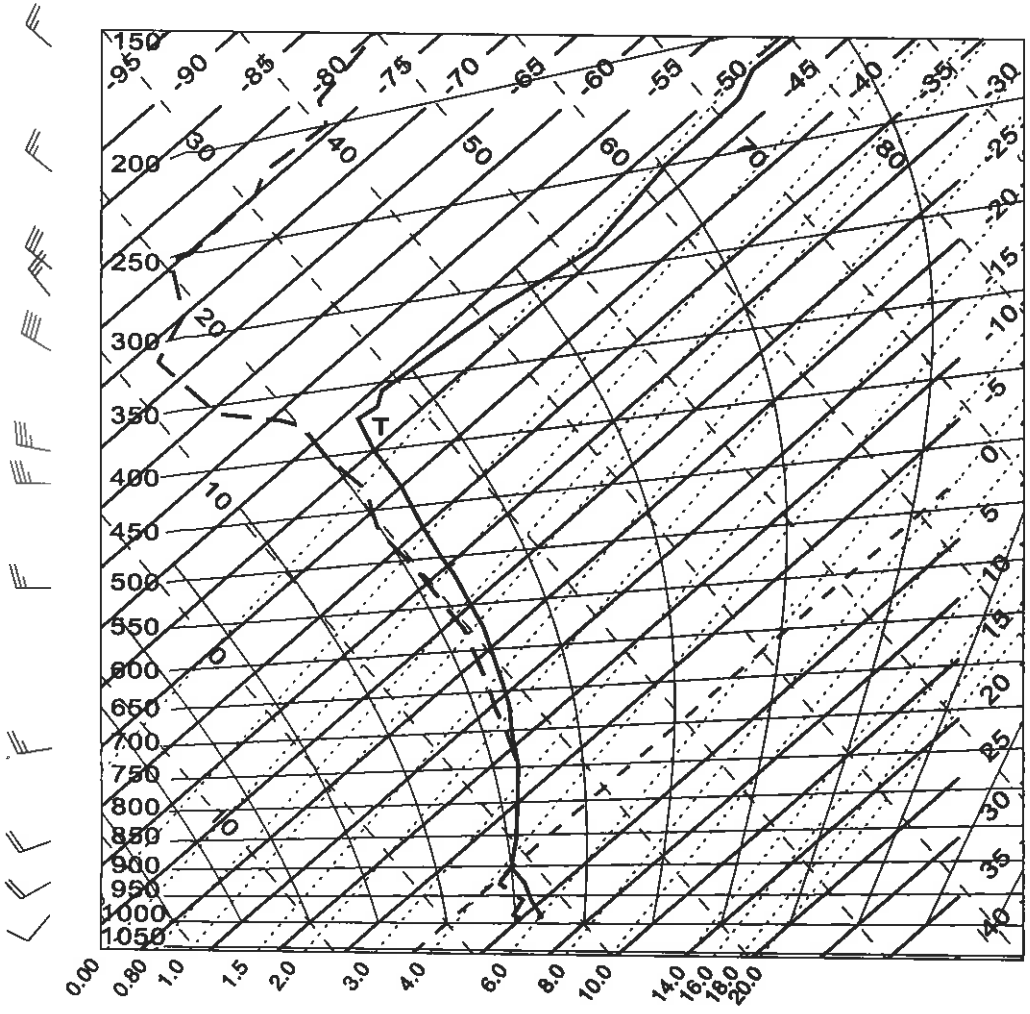

Fig 11a

(b) Aberporth Radiosonde
26/01/99 17Z

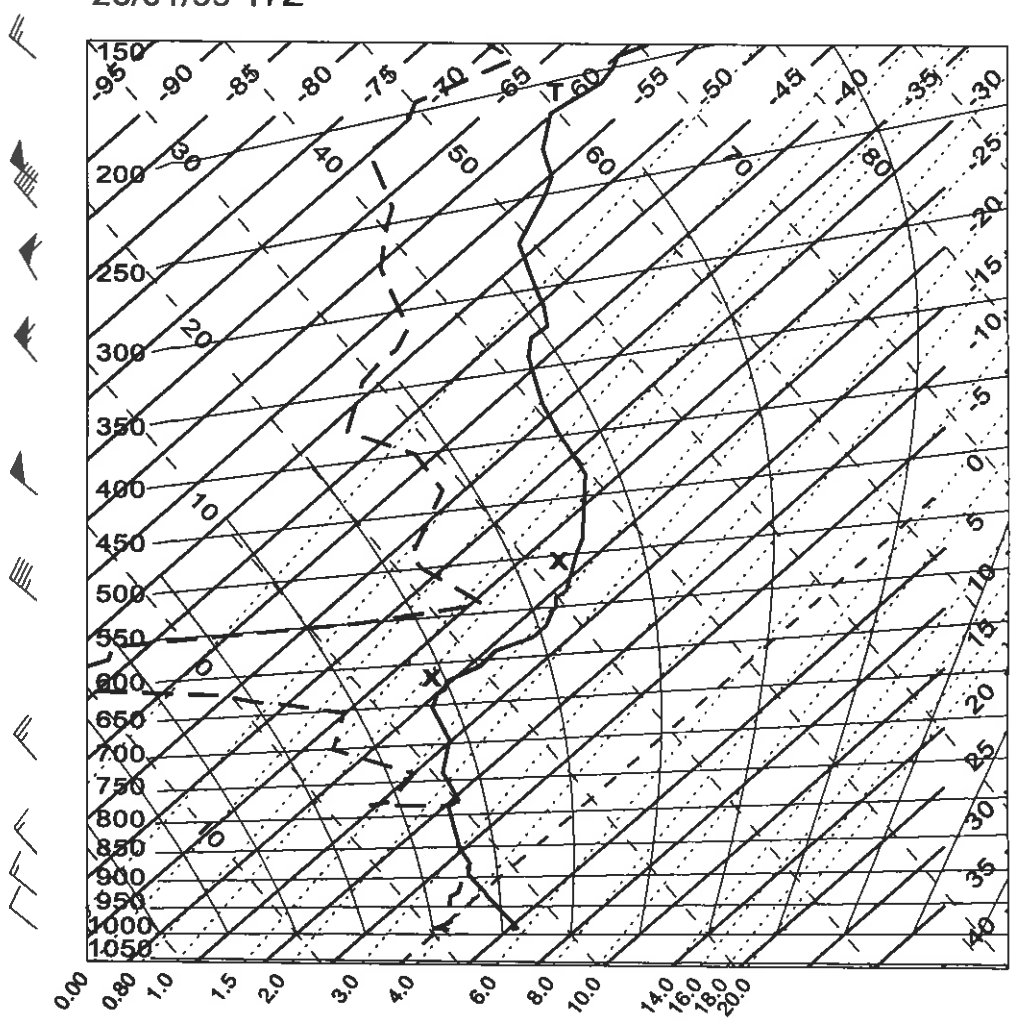

Fig 11b

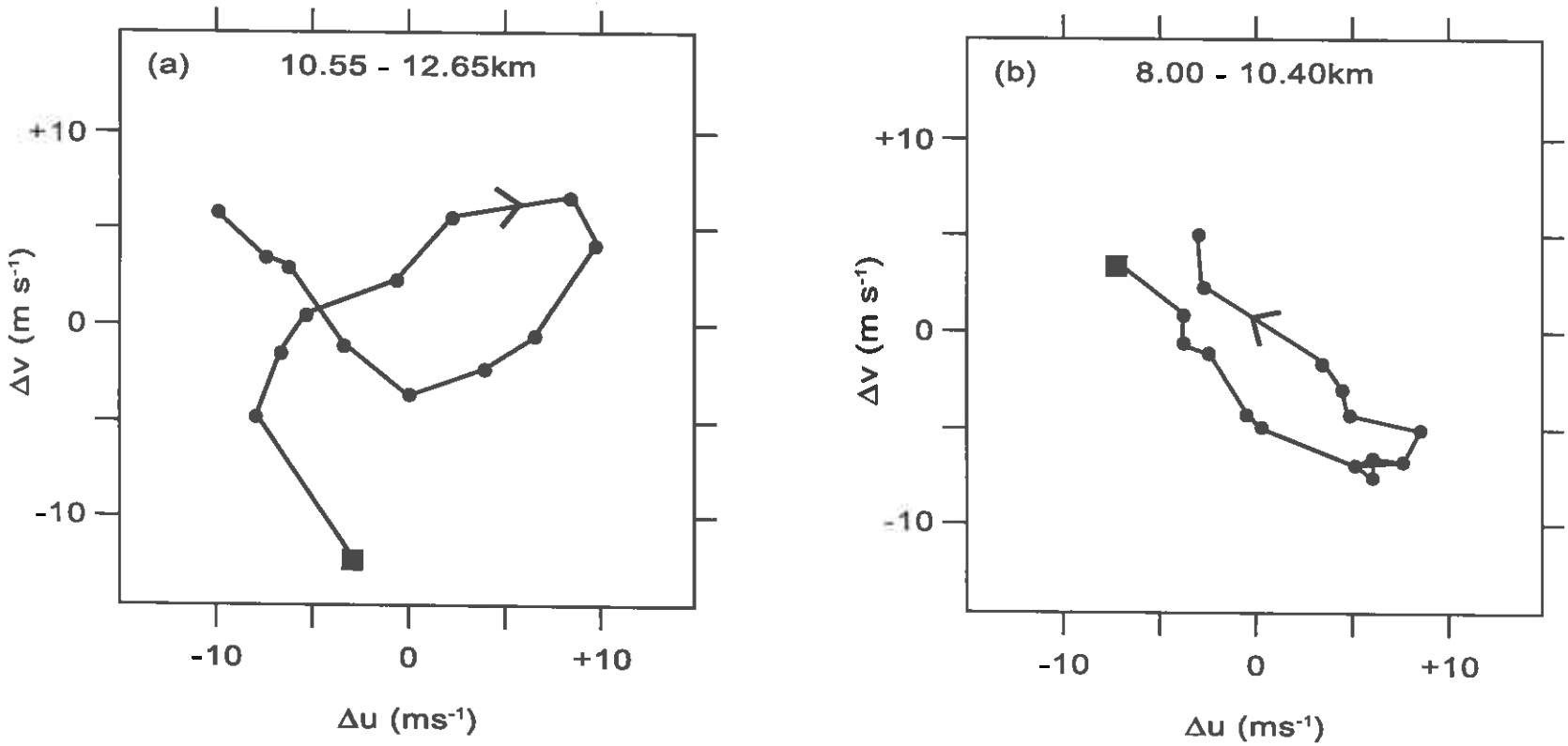
(a)
10.55 - 12.65km
+10
0
-10
Δv (m s-1)
-10
0
+10
Δu (ms-1)
(b)
8.00 - 10.40km
+10
0
-10
Δv (m s-1)
-10
0
+10
Δu (ms-1)

Fig 12

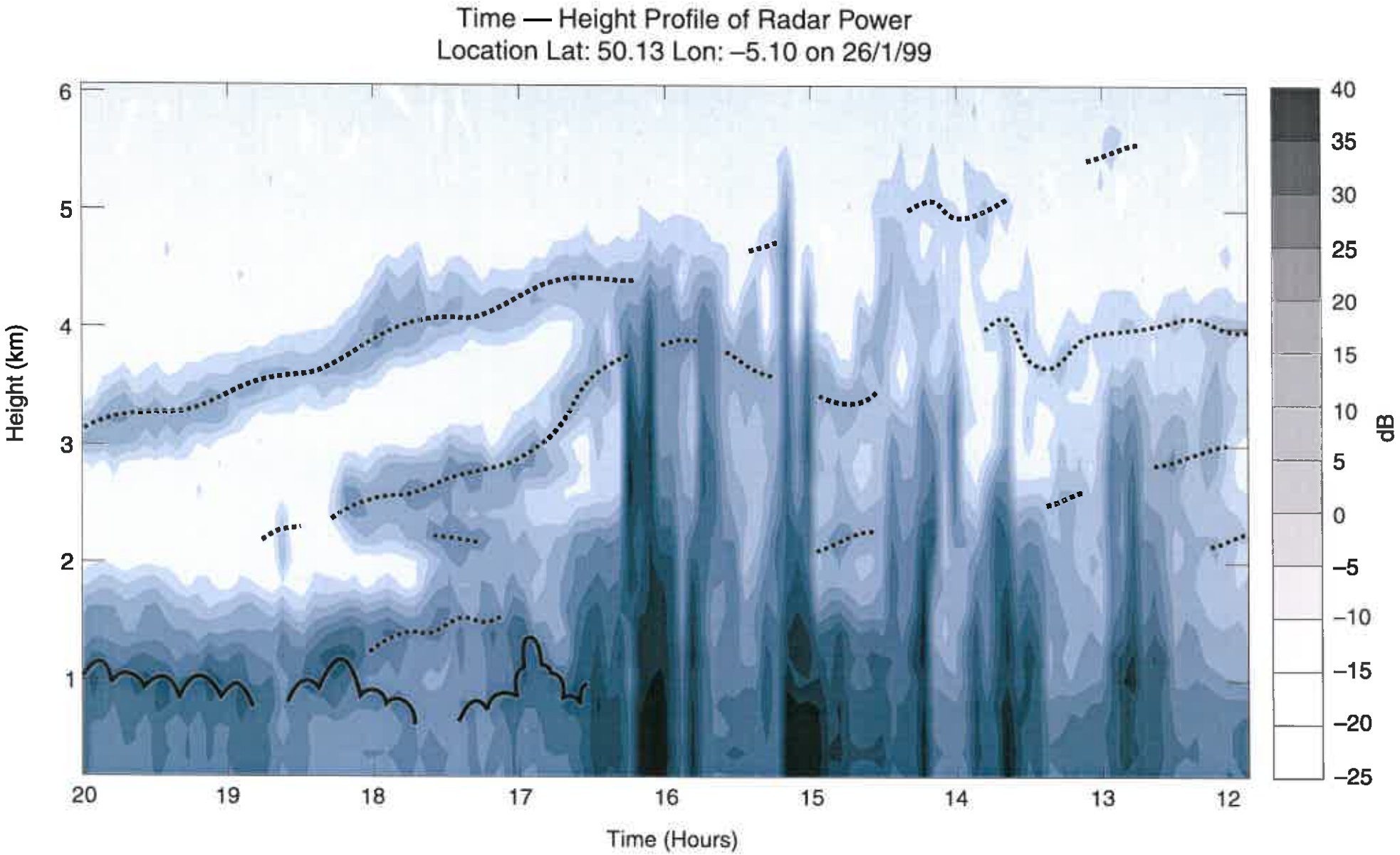
Time — Height Profile of Radar Power
Location Lat: 50.13 Lon: –5.10 on 26/1/99
Height (km)
6
5
4
3
2
1
20
19
18
17
16
15
14
13
12
Time (Hours)
40
35
30
25
20
15
10
5
0
–5
–10
–15
–20
–25
dB

Fig 13

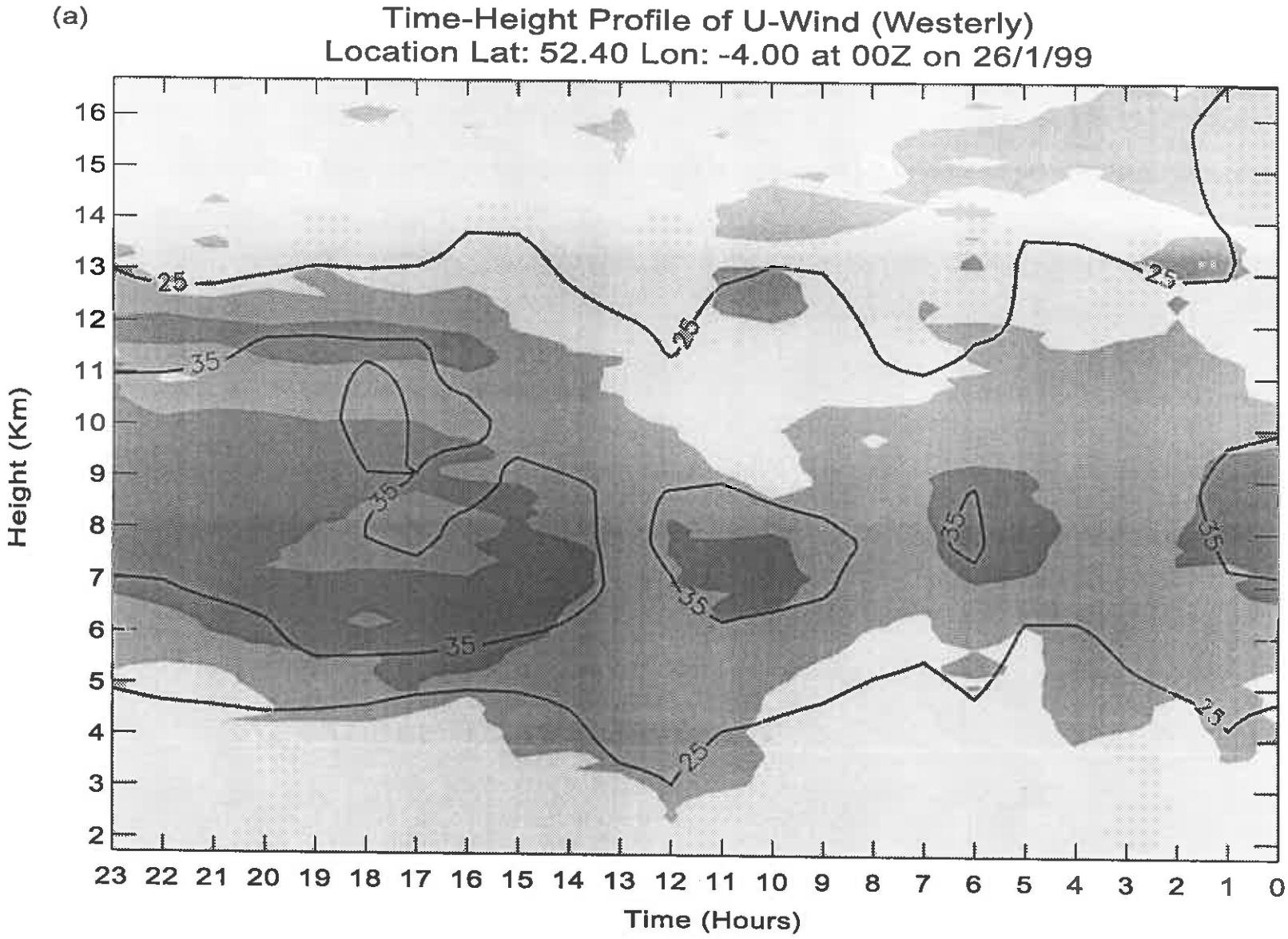
(a)
Time-Height Profile of U-Wind (Westerly)
Location Lat: 52.40 Lon: -4.00 at 00Z on 26/1/99
Height (Km)
16
15
14
13
12
11
10
9
8
7
6
5
4
3
2
25
35
23 22 21 20 19 18 17 16 15 14 13 12 11 10 9 8 7 6 5 4 3 2 1 0
Time (Hours)

Fig 14a

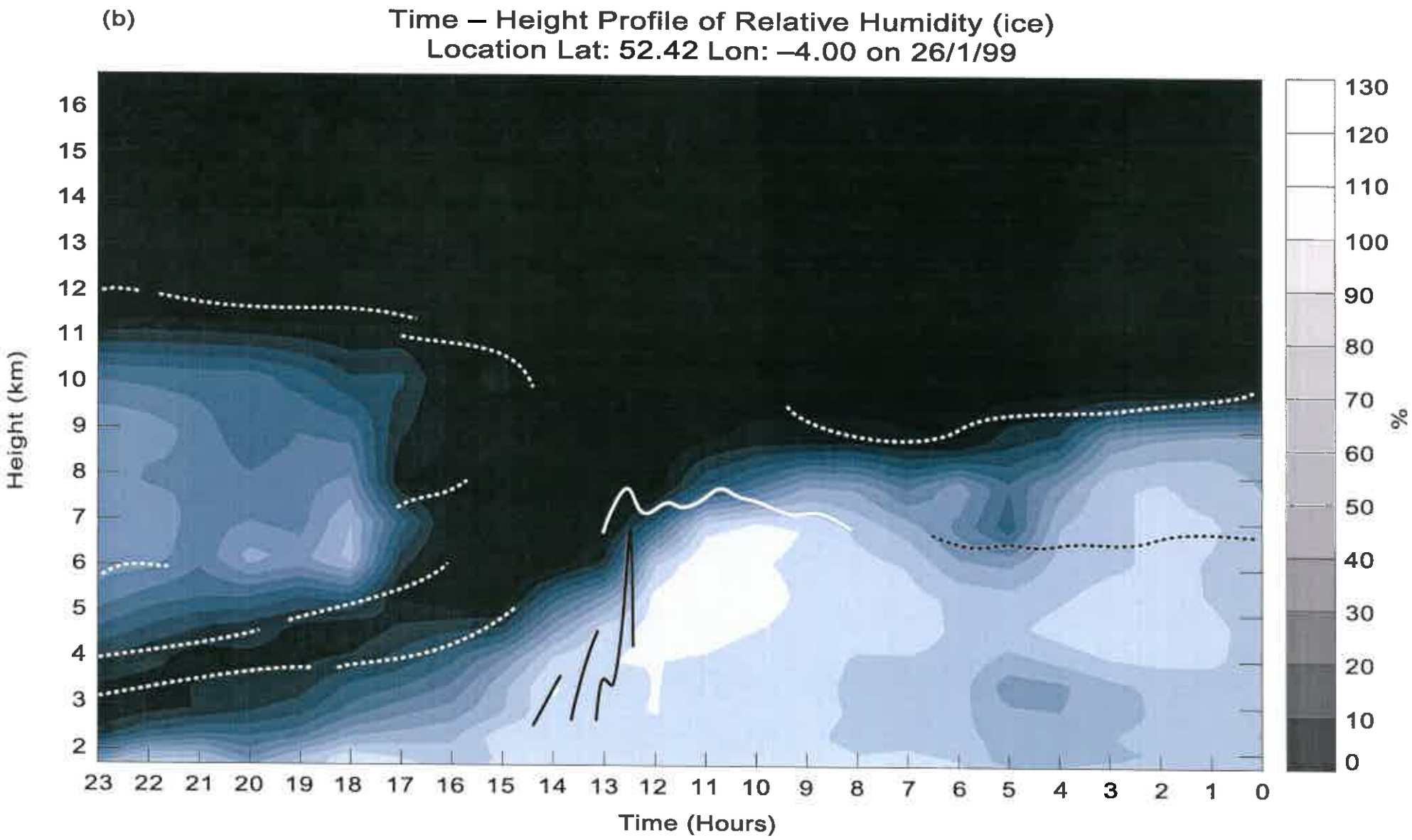
(b)
Time – Height Profile of Relative Humidity (ice)
Location Lat: 52.42 Lon: –4.00 on 26/1/99
Height (km)
16
15
14
13
12
11
10
9
8
7
6
5
4
3
2
23 22 21 20 19 18 17 16 15 14 13 12 11 10 9 8 7 6 5 4 3 2 1 0
Time (Hours)
130
120
110
100
90
80
70
60
50
40
30
20
10
0
%

Fig 14b

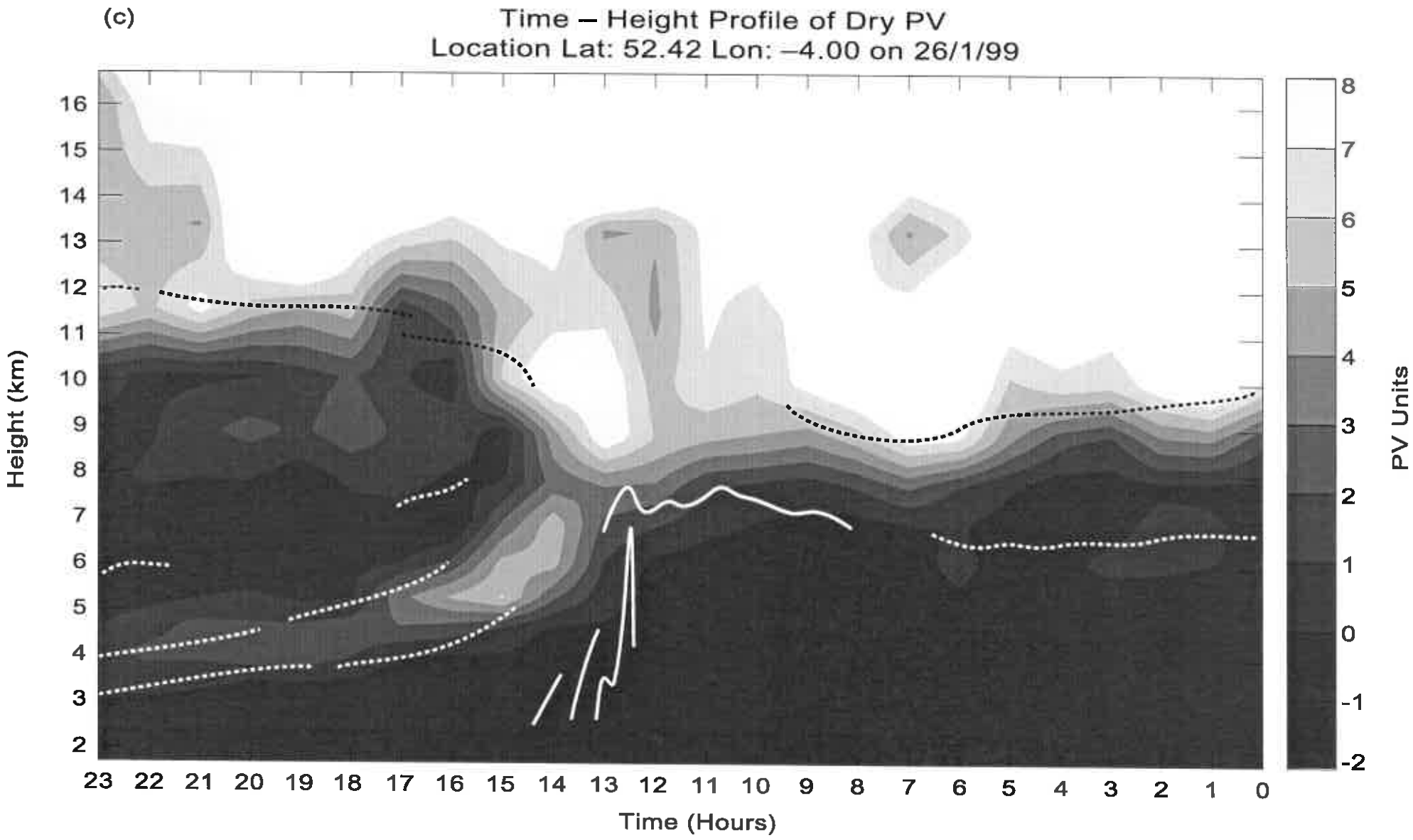
(c)
Time – Height Profile of Dry PV
Location Lat: 52.42 Lon: –4.00 on 26/1/99
Height (km)
16
15
14
13
12
11
10
9
8
7
6
5
4
3
2
23 22 21 20 19 18 17 16 15 14 13 12 11 10 9 8 7 6 5 4 3 2 1 0
Time (Hours)
PV Units
8
7
6
5
4
3
2
1
0
-1
-2

Fig 14c

(a)

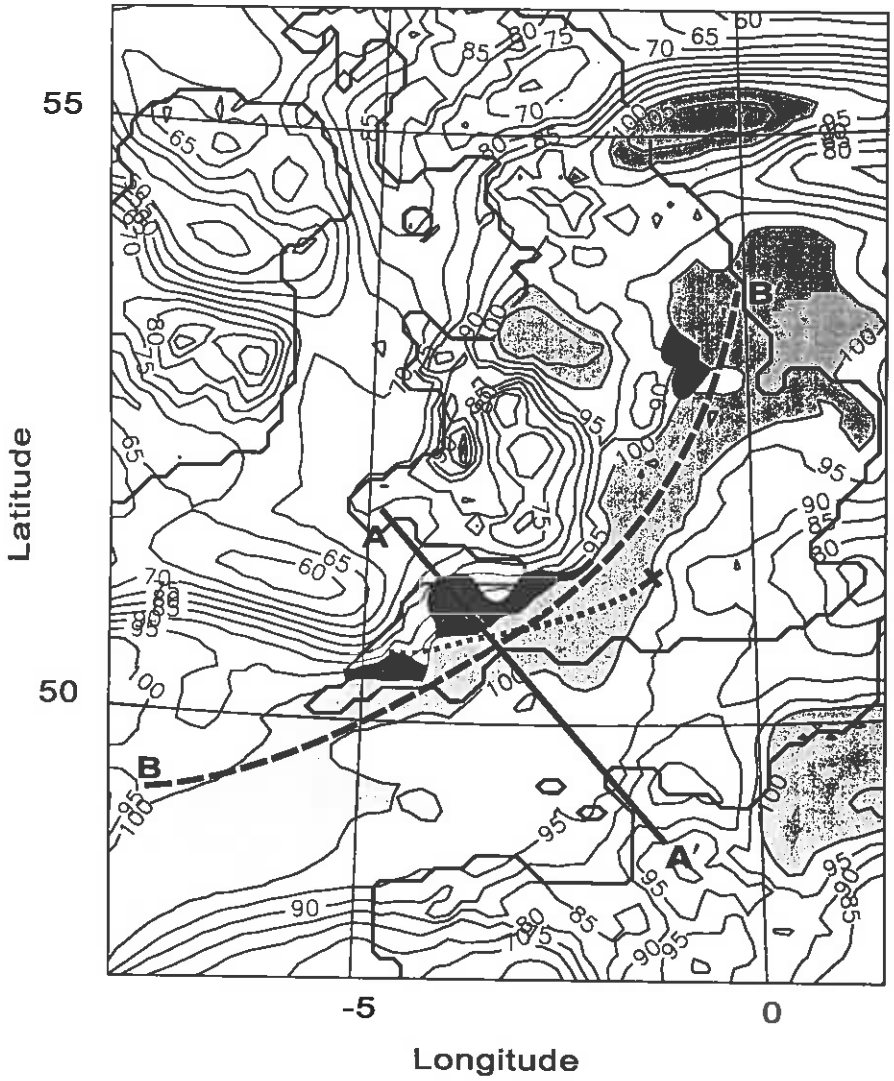

Fig 15a

(b)

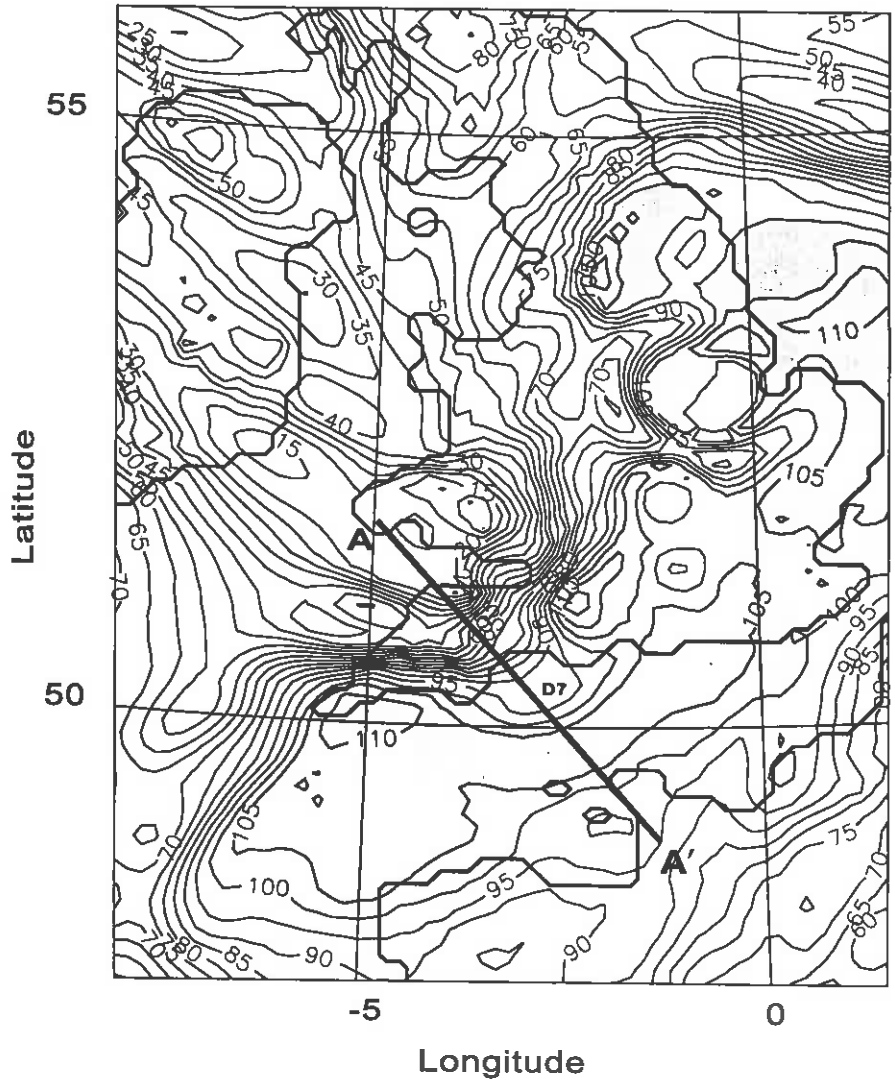

Fig 15b

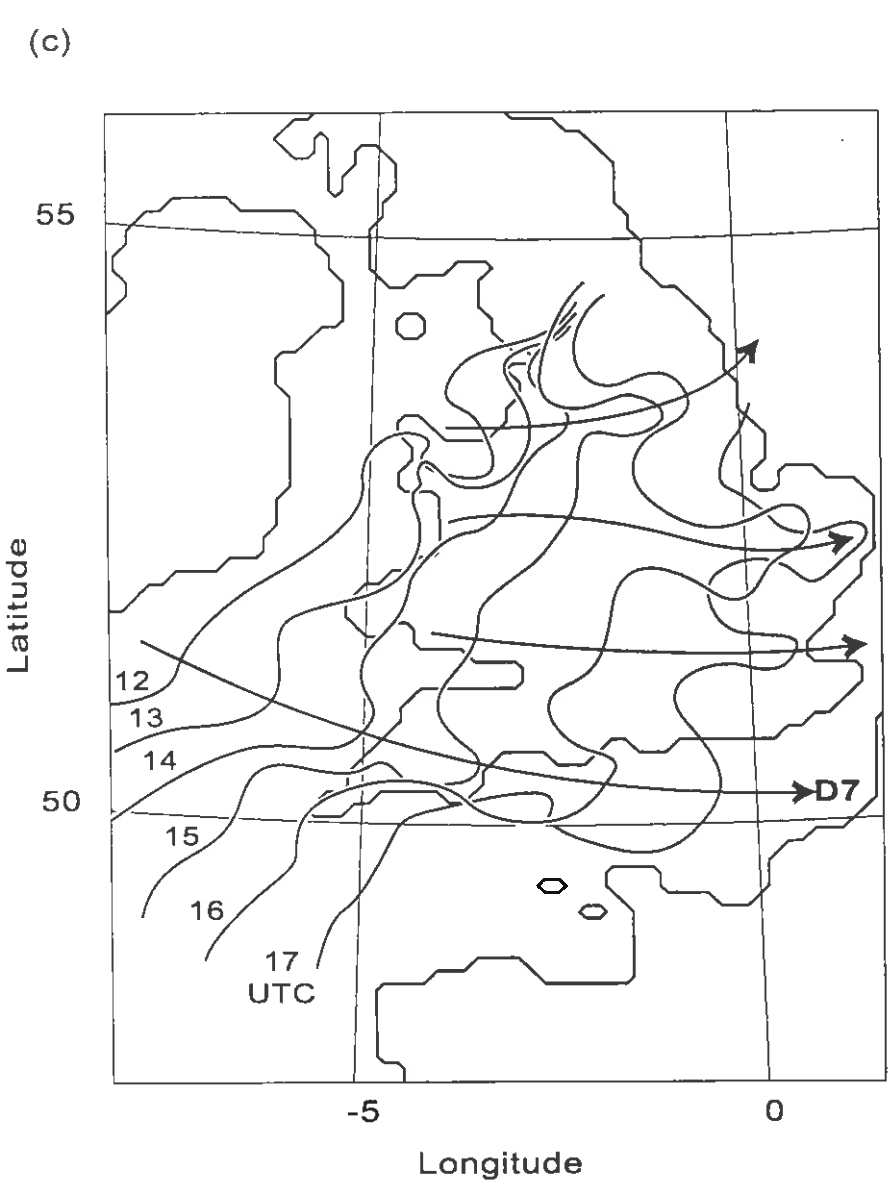

Fig 15c

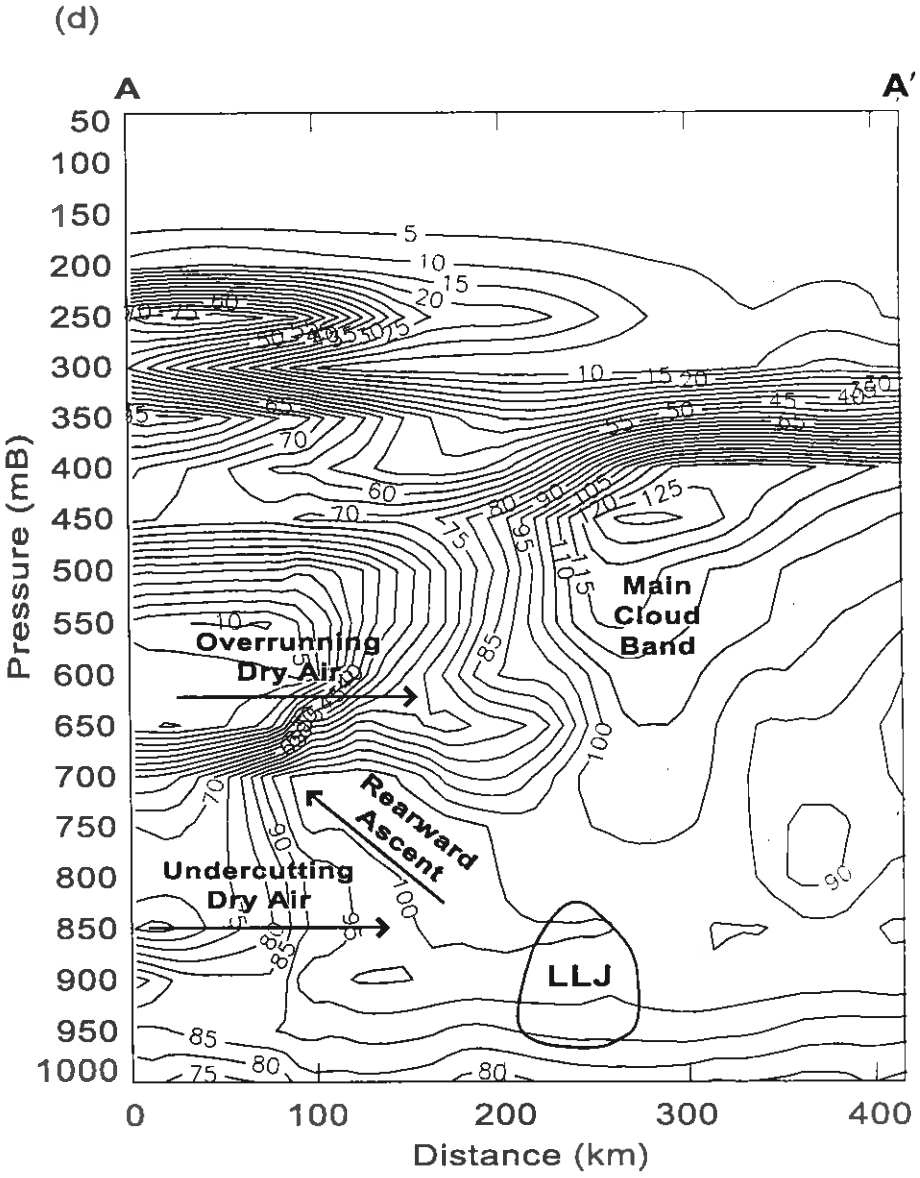

Fig 15d

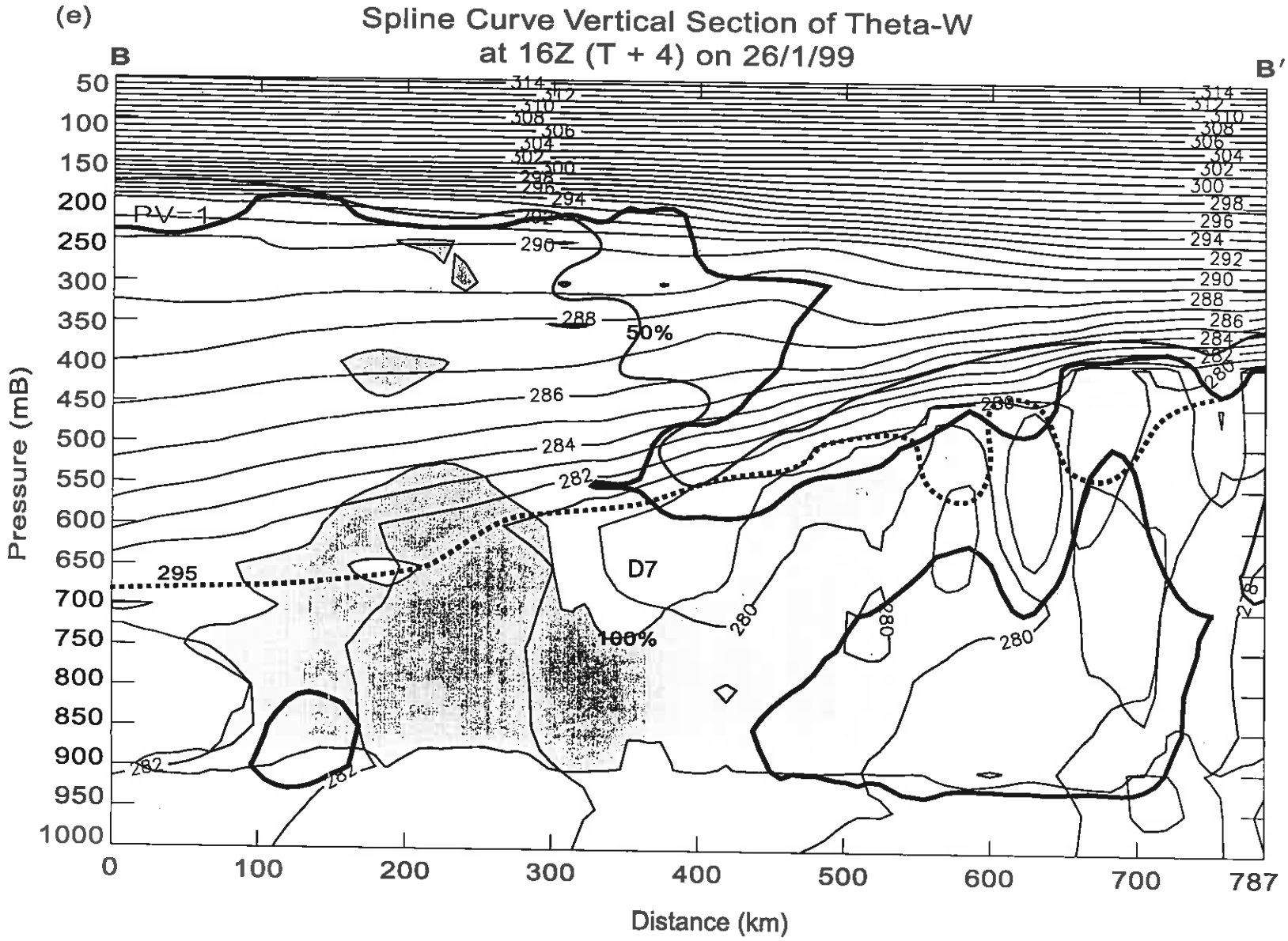
(e)
Spline Curve Vertical Section of Theta-W
at 16Z (T + 4) on 26/1/99
B
B'
Pressure (mB)
Distance (km)
PV=1
50%
100%
D7
295
50
100
150
200
250
300
350
400
450
500
550
600
650
700
750
800
850
900
950
1000
0
100
200
300
400
500
600
700
787

Fig 15e

CURRENT JCMM INTERNAL REPORTS

This series of JCMM Internal Reports, initiated in 1993, contains unpublished reports and also versions of articles submitted for publication. The complete set of Internal Reports is available from the National Meteorological Library on loan, if required.

1. **Research strategy and programme**
   K A Browning et al
   January 1993

2. **The GEWEX Cloud System Study (GCSS)**
   GEWEX Cloud System Science Team
   January 1993

3. **Evolution of a mesoscale upper tropospheric vorticity maximum and comma cloud from a cloud-free two dimensional potential vorticity anomaly**
   K A Browning
   January 1993

4. **The global energy and water cycle**
   K A Browning
   July 1993

5. **Structure of a midlatitude cyclone before occlusion**
   K A Browning and N Roberts
   July 1993

6. **Developments in systems and tools for weather forecasting**
   K A Browning and G Szejwach
   July 1993

7. **Diagnostic study of a narrow cold frontal rainband and severe winds associated with a stratospheric intrusion**
   K A Browning and R Reynolds
   August 1993

8. **Survey of perceived priority issues in the parametrizations of cloud-related processes in GCMs**
   K A Browning
   September 1993

9. **The effect of rain on longwave radiation**
   I Dharssi
   September 1993

10. **Cloud microphysical processes - a description of the parametrization used in the large eddy model**
    H Swann
    October 1993

11. **An appreciation of the meteorological research of Ernst Kleinschmidt**
    A J Thorpe
    May 1992

12. **Potential vorticity of flow along the Alps**
    A J Thorpe, H Volkert and Dietrich Heimann
    August 1992

13. **The representation of fronts**
    A J Thorpe
    January 1993

14. **A parametrization scheme for symmetric instability: test for an idealised flow**
C S Chan and A J Thorpe
February 1993

15. **The Fronts 92 Experiment: a Quicklook Atlas**
Edited by T D Hewson
November 1993

16. **Frontal wave stability during moist deformation frontogenesis**
Part 1: Linear wave dynamics
C H Bishop and A J Thorpe
May 1993

17. **Frontal wave stability during moist deformation frontogenesis**
Part 2. The suppression of non-linear wave development
C H Bishop and A J Thorpe
May 1993

18. **Gravity waves in sheared ducts**
S Monserrat and A J Thorpe
October 1993

19. **Potential vorticity and the electrostatics analogy: quasi-geostrophic theory**
C Bishop and A J Thorpe
November 1993

20. **Recent advances in the measurement of precipitation by radar**
A J Illingworth
April 1993

21. **Micro-physique et givrage: cloud microphysics and aircraft icing**
A J Illingworth
May 1993

22. **Differential phase measurements of precipitation**
M Blackman and A J Illingworth
May 1993

23. **Estimation of effective radius of cloud particles from the radar reflectivity**
N I Fox and A J Illingworth
May 1993

24. **A simple method of Dopplerising a pulsed magnetron radar**
A Hua, A J Illingworth and J Eastment
November 1993

25. **Radiation and polar lows**
George C Craig
February 1994

26. **Collected preprints submitted to the International Symposium on the Life Cycles of Extratropical Cyclones; Bergen, Norway, 27 June - 1 July 1994**
April 1994

27. **Convective frontogenesis**
Douglas J Parker and Alan J Thorpe
April 1994

28. **Improved measurement of the ice water content in cirrus using a total water evaporator**
Philip R A Brown and Peter N Francis
April 1994

29. **Mesoscale effects of a dry intrusion within a vigorous cyclone**
K A Browning and B W Golding
April 1994

30. **GEWEX Cloud System Study, Science Plan**
May 1994

31. **Parametrization of momentum transport by convectively generated gravity waves**
R Kershaw
May 1994

32. **Mesoscale Modelling Newsletter No 5**
May 1994

33. **Observations of the mesoscale sub-structure in the cold air of a developing frontal cyclone**
K A Browning, S A Clough, C S A Davitt, N M Roberts and T D Hewson
May 1994

34. **Longwave radiative forcing of a simulated tropical squall line**
Imtiaz Dharssi
July 1994

35. **On the nature of the convective circulation at a kata-cold front**
K A Browning
September 1994

36. **Collective preprints of papers submitted to the COST-75 International Seminar on Advanced Weather Radar Systems, Brussels, 20-23 September 1994**
November 1994

37. **Use of satellite imagery to diagnose events leading to frontal thunderstorms: Parts I and II of a case study**
K A Browning and N M Roberts
November 1994

38. **The role of spaceborne millimetre-wave radar in the global monitoring of ice cloud**
P R A Brown, A J Illingworth, A J Heymsfield, G M McFarquhar, K A Browning and M Gosset
December 1994

39. **Potential vorticity inversion**
Michal Ziemianski
October 1994

40. **Theory of mature tropical cyclones; a comparison between Kleinschmidt (1951) and Emanuel (1986)**
Suzanne L Gray
December 1994

41. **Dispersion and removal of pollutants during the passage of an atmospheric frontal system**
N R Gimson
December 1994

42. **The role of snow sublimation in frontogenesis**
D J Parker and A J Thorpe
December 1994

43. **Potential vorticity and the electrostatics Analogy: Ertel-Rossby formulation**
A J Thorpe and C H Bishop
December 1994

44. **Mesoscale aspect of extratropical cyclones: an observational perspective**
K A Browning
January 1995

45. **A polar low outbreak: evolution and mesoscale structures**
T D Hewson, G C Craig and C Claud
February 1995

46. **Generation of near-surface gusts of deep convection**
K Nakamura and R Kershaw
April 1995

47. **Attribution concepts applied to the Omega Equation**
S A Clough, C S A Davitt and A J Thorpe
June 1995

48. **Parametrization of mixed-phase cloud and precipitation**
Susan P Ballard and M Gerard Hutchinson
June 1995

49. **Short-range forecasting of stratocumulus: initialization prediction**
Susan P Ballard, Simon D Jackson and B Macpherson
June 1995

50. **Contributions of the JCMM/Dept of Meteorology Radar Group to the 27th AMS Radar Meteorology Conference, Vail October 1995**
June 1995

51. **Cold pools in shear**
Douglas J Parker
September 1995

52. **High-resolution analysis of frontal fracture**
K A Browning, S P Ballard and C S A Davitt
September 1995

53. **The albedo of broken cloud fields: calculations using a modified two stream radiation code**
Imtiaz Dharssi and Roy Kershaw
October 1995

54. **Parametrization of momentum transport by convection. I: theory and cloud modelling results**
R Kershaw and D Gregory
November 1995

55. **Variation of frontal structure along a cold front**
K A Browning and N M Roberts
November 1995

56. **Secondary frontal waves**
Douglas Parker
December 1995

57. **Objective fronts**
T D Hewson
March 1996

58. **Mesoscale analysis of the activation of a cold front during cyclogenesis**
K A Browning, N M Roberts and A J Illingworth
June 1996

59. **Investigation of different representations of rain in a 1-d evaporation model**
H Swann
May 1996

60. **Parametrization of diabatic processes in the inversion of the omega-equation**
M Athanassiadou and A J Thorpe
June 1996

61. **The role of the environmental flow in the development of secondary frontal cyclones**
I A Renfrew, A J Thorpe and A Joly
June 1996

62. **Consequences of the geostrophic momentum approximation on barotropic instability**
S Malardel, A J Thorpe and A Joly
June 1996

63. **Contributions to the AMS/RMS Conference on Mesoscale Processes**
Reading, 9-13 September 1996

64. **Vorticity and potential vorticity in stratified flows interacting with an isolated obstacle**
Jorge A Gutiérrez and A J Thorpe
September 1996

65. **Triple point development: two case studies**
Douglas Parker
September 1996

66. **Radar observations of wind-shear splitting within evolving atmospheric Kelvin-Helmholtz billows**
D Chapman and K A Browning
April 1997

67. **Cold frontal structure derived from radar wind profilers**
K A Browning, D Jerrett, J Nash, T Oakley and N M Roberts
May 1997

68. **The dry intrusion and its effect on the frontal, cloud and precipitation structure of extratropical cyclones**
K A Browning - Text of invited special lecture at the Spring Conference
of the Meteorological Society of Japan, University of Tsukuba, 22 May 1997

69. **Met. Office Unified Model data, diagnostics, graphics programs, and other observational data available from the JCMM through the aegis of the Universities Weather Research Network (UWERN).** (Plus supplement)
Peter Panagi and Ed Dicks
June 1997

70. **Contributions of the JCMM/Dept of Meteorology Radar Group to the 28th AMS Radar Meteorology Conference.** Austin, Texas
September 1997

71. **Sensitivity of short-range weather forecasts to local potential vorticity modifications**
Meral Demirtas and Alan Thorpe
July 1997

72. **Objective identification of frontal wave cyclones**
T D Hewson
August 1997

73. **Attribution and its application to mesoscale structure associated with tropopause folds**
A J Thorpe
September 1997

74. **The role of the environmental flow in the development of secondary frontal cyclones**
Ian A Renfrew, Alan J Thorpe and Craig H Bishop
September 1997

75. **Potential vorticity: a short history of its definitions and uses**
Alan J Thorpe and Hans Volkert
September 1997

76. **Superposing semi-geostrophic potential vorticity anomalies**
H R Birkett and A J Thorpe
September 1997

77. **Short period forecasting of catchment-scale precipitation.**
Part 1: the role of Numerical Weather Prediction
M A Pedder, M Haile and A J Thorpe
September 1997

78. **Verification of the tracking technique used in an experimental cloud motion wind inferring system**
Z Wang, K A Browning and G A Kelly
October 1997

79. **A preliminary study of Fourier series analysis for cloud tracking with GOES high temporal resolution images**
Z Wang
October 1997

80. **Analysis of an ex-tropical cyclone after reintensifying as a warm-core extratropical cyclone**
K A Browning, G Vaughan and P Panagi
November 1997

81. **A JCMM overview of FASTEX IOPs**
S A Clough, H W Lean, N M Roberts, H Birkett, J-P Chaboureau, R Dixon, M Griffiths, T D Hewson and A Montani
January 1998

82. **Programs for PV inversion and modification**
Meral Demirtas
December 1997

83. **Release of potential shearing instability in warm frontal zones**
D Chapman and K A Browning
February 1998

84. **The European Cloud-Resolving Modelling Programme (EUCREM)**
Summary Report from the coordinator
P W White
April 1998

85. **A frontal wave database**
T D Hewson
April 1998

86. **Layering observed in dropsoundings from IOP 1 of Fronts 92**
S A Clough
May 1998

87. **Use of wind-shear displays for Doppler radar data**
D Chapman and K A Browning
May 1998

88. **Radar estimates of rainfall rates at the ground in bright band and non-bright band events**
T J Smyth and A J Illingworth
June 1998

89. **Correction for attenuation of radar reflectivity using polarisation data**
T J Smyth and A J Illingworth
June 1998

90. **The effects of convection on chemical reactions and precipitation scavenging**
Neil R Gimson
July 1998

91. **How to use the display program DISP**
Nigel Roberts
August 1998

92. **Conceptual models of cyclogenesis**
Adrian T Semple
August 1998

93. **Observations of oblate hail using dual polarisation radar and implications for hail detection schemes**
T J Smyth, T M Blackman and A J Illingworth
September 1998

94. **The semigeostrophic diagnosis of vertical motion. Part I: Formulation and co-ordinate transformations**
Mike A Pedder and Alan J Thorpe
September 1998

95. **The semigeostrophic diagnosis of vertical motion. Part II: Results for an idealised baroclinic wave life cycle**
Alan J Thorpe and Mike A Pedder
September 1998

96. **Convective destabilisation by a tropopause fold diagnosed using potential vorticity inversion**
Morwenna Griffiths, Alan Thorpe and Keith Browning
October 1998

97. **Forecast skill of the ECMWF model using targeted observations during FASTEX**
A Montani, A J Thorpe, R Buizza and P Unden
October 1998

98. **Observations and model simulations of the FASTEX IOP 16 frontal wave - effects of sublimation**
Sid A Clough, Humphrey W Lean, Nigel M Roberts and Richard M Forbes
December 1998

99. **The application of conceptual models in NWP**
Adrian T Semple
January 1999

100. **Mesoscale analysis of arc rainbands in a dry slot**
K A Browning and N M Roberts
January 1999

101. **Interaction of mesoscale tropopause depressions with a warm-core cyclone: observational and model analyses, and sensitivity to analysis errors**
K A Browning, A J Thorpe, A Montani, D Parsons, M Griffiths, P Panagi and E M Dicks
February 1999

102. **The use of water vapour imagery and PV inversion to adjust initial conditions in NWP**
Sean J Swarbrick
February 1999
This report is no longer available; see Internal Report No.108

103. **Summary notes for a lecture course on Waves in the Atmosphere and Ocean**
A A White
March 1999

104. **Results of a questionnaire on the operational value of conceptual models (CMs) of fronts and cyclones**
N M Roberts & M V Young
July 1999

105. **Contributions to the Poster Session at the 1998 UWERN Annual Science Meeting**
assembled by A A White
August 1999

106. **The objective analysis of dropsonde data from FASTEX**
Richard Forbes, Sid Clough, Mark Dixon, Andy Macallan & Nigel Roberts
January 2000

107. *NWP Technical Report No.302*
Implications for Mesoscale Modelling from a Study of the FASTEX IOP 16 Mid-latitude Cyclone
Richard M Forbes, Humphrey W Lean, Nigel M Roberts and Peter A Clark
March 2000

108. *NWP Technical Report No.291*
The use of water vapour imagery and PV inversion to adjust initial conditions in NWP
Final Project Report
Sean J Swarbrick
September 1999

109. *NWP Technical Report No.294*
A guide to aspects of water vapour imagery interpretation: the significance of dry regions
Nigel M Roberts
January 2000

110. *NWP Technical Report No.300*
The relationship between water vapour imagery and thunderstorms
Nigel M Roberts
February 2000

111. *NWP Technical Report No.293*
Holomorphic structures in hydrodynamical models of nearly geostrophic flow
V N Roubtsov and I Roulstone
January 2000

112. *NWP Technical Report No.301*
Multi-sensor synthesis of the mesoscale structure of a cold-air comma cloud system
K A Browning, P Panagi and E M Dicks
March 2000

Met Office Joint Centre for Mesoscale Meteorology Department of Meteorology
University of Reading PO Box 243 Reading RG6 6BB United Kingdom
Tel: +44 (0)118 931 8425 Fax: +44 (0)118 931 8791
www.metoffice.com